

The boundary layer in the scale-relativity theory of turbulence

Cite as: Phys. Fluids **36**, 065133 (2024); doi: [10.1063/5.0212386](https://doi.org/10.1063/5.0212386)

Submitted: 4 April 2024 · Accepted: 18 May 2024 ·

Published Online: 14 June 2024



View Online



Export Citation



CrossMark

Laurent Nottale^{a)}  and Thierry Lehner^{b)} 

AFFILIATIONS

Laboratoire Univers et Théories, Observatoire de Paris Université PSL, CNRS, Université Paris Cité, F-92195 Meudon Cedex, France

^{a)}Electronic mail: laurent.nottale@obspm.fr

^{b)}Author to whom correspondence should be addressed: thierry.lehner@obspm.fr

ABSTRACT

We apply the scale-relativity theory of turbulence to the turbulent boundary layer problem. On the basis of Kolmogorov's scaling, the time derivative of the Navier–Stokes equations can be integrated under the form of a macroscopic Schrödinger equation acting in velocity-space. In this equation, the potential coming from pressure gradients takes the form of a quantum harmonic oscillator (QHO) in a universal way. From the properties of QHOs, we can then derive the possible values of the ratio of turbulent intensities in the shear flow, $R = \sigma_u/\sigma_v = 1.35 \pm 0.05$. We show that the Karman constant is theoretically predicted to be $\kappa = 1/R^3$, in good agreement with its typical value $\kappa \approx 0.4$ and its observed possible variations. Then, we find a generic solution of our equations for the normal Reynolds stress pure profile, which closely fits the data from laboratory and numerical experiments. Its amplitude, μ_B , is the solution of an implicit equation that we solve numerically and analytically through power series, yielding to lowest order $\mu_B - 1.35 \approx -2(R - 1.35)$, plus smaller contributions from other parameters. Consequently, the correlation coefficient of velocities is given by $\rho \approx 1/R\mu_B^2 \approx 1/R^3 \approx 0.4$ and is therefore equal to the Karman constant to lowest order, in agreement with its universally measured value ≈ 0.4 for all shear flows. We also find a general similarity between turbulent round jets and boundary layers in their outer region. These results therefore apply to a wide set of turbulent flows, including jets, plane boundary layers, and, to some extent, channels and pipes.

Published under an exclusive license by AIP Publishing. <https://doi.org/10.1063/5.0212386>

I. INTRODUCTION

In the study of turbulence, the plane boundary layer plays a prominent role since the solution of the mean flow based on the asymptotic matching of the inner and outer layers yields the very important result of the “log-law of the wall.”^{1,2} With the Kolmogorov scaling law (K41),³ this logarithmic velocity profile in the inertial sub-layer is indeed one of the major landmarks in turbulence theory. With analytical tools of a rather general nature, a very specific result has been obtained, even though the equations of motion cannot be solved in general.^{4,5} This approach became “classical” and was universally applied to all wall-bounded flows. The same logarithmic law and its parameters, in particular the Karman constant $\kappa \approx 0.4$ on which it depends, were considered valid for boundary layers, channels, and pipes. Laboratory and numerical experiments suggest that the Karman constant is universal, although with small possible variations of the order of $\sim 5\%$,^{6,7} which has led to question its strict universality.⁸

The log-law profile equation and its intrinsic Karman constant are widely used in fluid mechanics. However, despite numerous theoretical and empirical attempts to establish formal bases for these

concepts, no consensus has been reached.⁹ The log-law has been theoretically justified through many different arguments and has been advocated for a wide range of wall-bounded shear flows (see references in Refs. 6 and 9). The value of the Karman constant has been measured through numerous experiments and direct numerical simulations of Navier–Stokes equations (DNS).⁶ Many attempts of theoretical derivations have been made (see review in Ref. 9) but always from merely postulated models instead of the fluid mechanics equations. As a result, these theoretical derivations do not concur and the origin of its value remains elusive.

This difficulty can be traced back to a more fundamental and universal problem encountered up until now by all theories of turbulence: the closure problem. When a fluid becomes turbulent, its properties are described not only by the mean velocities but also by their fluctuations described by the Reynolds stresses. As a consequence, the number of equations is smaller than the number of unknowns and the present theory remains incomplete.

In a recent work,¹⁰ we have suggested a solution to this closure problem and applied it to turbulent jets by using the scale-relativity

approach to turbulence.^{11–13} This has allowed us to obtain theoretical understanding and predictions for the Reynolds stress profiles and for several universal dimensionless quantities, such as the jet opening angle $\alpha_j \approx 0.2$, the ratio $R \approx 1.35$ of turbulent intensity amplitudes along the radial direction over the axial one, the mean ratio $X \approx 1/4$ of turbulent intensities over the mean velocity on the jet centerline, and the correlation coefficient of velocities, which we have found to be given by $\rho = 1/R^3 \approx 0.4$.¹⁰

In the present paper, we apply the same approach to the turbulent plane boundary layer problem (far from the wall, i.e., in the zone where viscosity becomes negligible), so it will be relevant to fully developed channel flow, fully developed pipe flow, and the flow in a flat plate boundary layer. These simple flows are of practical importance and have played a prominent role in the historical development of the study of turbulent flows.⁵ Their description is part of basic textbook knowledge on turbulence,^{4,5,14,15} yet many features characterizing them remain empirical, in particular purely numerical constants such as the Karman constant.

Tennekes and Lumley⁴ have remarked that boundary layer flows are more complicated than flows in free shear layers (such as in our previous study of the free round jet) because the presence of a solid wall imposes constraints that are absent in wakes and jets. Shear flows are very important to understand turbulence, which is often described as just an instability generated by shear.

The dimensionless character of seemingly universal physical constants appearing in turbulence, such as the Karman constant for boundary layers, makes the understanding of their value one of the most fascinating problems in physics. Moreover, this question is clearly related to a more general problem in the theory of turbulence, namely, the closure problem: when jumping to a turbulent behavior, a fluid is described not only by its mean velocities, which are solutions of the continuity and Navier–Stokes equations, but also by the velocity fluctuations. In today's theory, there are no known first principles equations for the covariances of these fluctuations (Reynolds stress), which yet appear in the Reynolds averaged Navier–Stokes (RANS) equations, so the number of unknowns is larger than the number of equations. The closure is therefore obtained using hypothetical models.

The scale-relativity approach to turbulence^{10–13,16} is of a different nature. In this framework, the closing equations do not come from an assumed model. They just derive from a reformulation and an integration of the time derivative of the Navier–Stokes equations themselves, written in v -space and accounting for the non-differentiable and fractal nature of velocities in the turbulent regime at inertial scales (according to Kolmogorov K41 scaling). The main result of this approach is that these v -space NS-derived equations can be re-integrated under the form of a macroscopic Schrödinger equation.^{13,17,18} In this equation, the microscopic Planck constant, \hbar , is replaced by a new macroscopic constant, \hbar_v , resulting from the self-organization of the turbulent medium, that is proportional to the rate of dissipated energy ε . The square of the modulus of the wave function that is the solution of this equation, $P = |\psi|^2$, yields the probability density distribution (PDF) of turbulent velocity fluctuations, from which the Reynolds stresses can be calculated, thus solving the closure problem.

Moreover, the potential entering this v -Schrödinger equation is, in a universal way, that of a harmonic oscillator,^{10,16} so we can theoretically predict that the local velocity PDFs are that of quantized harmonic oscillators (QHOs), possibly damped (QDHOs). This

theoretical expectation has been well verified by an analysis of experimental data.¹³

In this paper, we first recall in Sec. II the governing equations for the shear flow, which include in our approach both the Reynolds averaged Navier–Stokes (RANS) equations in the boundary layer approximation and the v -space macroscopic Schrödinger equation derived from the Navier–Stokes equations in the turbulent regime. In Sec. III, we recall some well-known basic theoretical results concerning the turbulent boundary layer, such as the log-law of the wall involving the Karman constant and the derivation of the Reynolds shear stress profile from the RANS equations. In Sec. IV, we recall our theoretical prediction for the possible values of the turbulent intensity ratio $R = \sigma_u/\sigma_v = 1.35 \pm 0.03$ far from the wall, which is similar to its derivation for the round jet¹⁰ from the general properties of QHOs. Then, we give in Sec. V a general physics argument leading to the conclusion that the Karman constant is given by $\kappa = R^{-3}$, which agrees with its values measured in laboratory and numerical experiments. The pure (normalized) profile of the normal Reynolds stress, σ_v^2 , is derived in Sec. VI from the normal component of the v -Schrödinger equation in a QHO potential. In Sec. VII, an implicit equation is found for its amplitude, μ_B^2 , from the uv component of the v -Schrödinger equation. We solve this equation both numerically and analytically through power series, thus obtaining an expression for μ_B in function of R , with smaller dependence on other parameters. Then, we show in Sec. VIII that, applying relevant scaling factors, the turbulent round jet and the turbulent boundary layer become similar in the region $z > \approx 0.2$, where $z = y/\delta$ in the boundary layer and $z = r/\alpha x$ in the jet, being described by the same equations. In Sec. IX, we finally suggest a solution for the puzzle concerning the value of the coefficient of correlation of velocities, which is found in observations, experiments, and direct numerical simulations to be universally equal to $\rho \approx 0.4$ for all shear flows. These results are discussed in Sec. X while Sec. XI is dedicated to the conclusion.

II. GOVERNING EQUATIONS FOR THE TURBULENT BOUNDARY LAYER

A. RANS equations

We shall study in the present paper the turbulent boundary layer that appears upon a flat plate subjected to a plane flow parallel to the wall. Such a flow is a particular case of a more general ensemble including channels and pipes.

We consider here only the two Cartesian coordinates x along the wall in the direction of the incident flow and y normal to the wall. We use the Reynolds decomposition of velocities $U_i = U + u$, $V_i = V + v$, where $U(x, y)$ and $V(x, y)$ are their average values and u, v their turbulent fluctuations. The fluid mechanics equations for the boundary layer consist of the continuity equation for the mean velocities,

$$\partial_x U + \partial_y V = 0, \quad (1)$$

and of the Reynolds averaged Navier–Stokes (RANS) equations:

$$x\text{RANS: } U \partial_x U + V \partial_y U + \partial_x (\bar{p} + \sigma_u^2) + \partial_y \sigma_{uv} - \nu \Delta U = 0, \quad (2)$$

$$y\text{RANS: } U \partial_x V + V \partial_y V + \partial_y (\bar{p} + \sigma_v^2) + \partial_x \sigma_{uv} - \nu \Delta V = 0, \quad (3)$$

where \bar{p} is the average pressure, $\sigma_u^2 = \langle u^2 \rangle$, $\sigma_v^2 = \langle v^2 \rangle$, and $\sigma_{uv} = \langle uv \rangle$ the Reynolds stresses and where we have taken $\rho = 1$ for simplification owing to the assumed incompressibility of the fluid.

In the so-called “boundary layer approximation,” the terms $\nu \partial_x \partial_x U$, $U \partial_x V$, $V \partial_y V$, and $\nu \Delta V$ are neglected. Moreover, in the turbulent case one may neglect the axial derivative of the Reynolds stresses on the grounds that they are small compared with the lateral gradients.⁵ One obtains

$$U \partial_x U + V \partial_y U = \nu \partial^2 U / \partial y^2 - \partial_y \sigma_{uv} - \partial_x (p_0 + \sigma_u^2 - \sigma_v^2) = 0, \tag{4}$$

$$\bar{p} = p_0(x) - \sigma_v^2. \tag{5}$$

These equations apply to all plane two-dimensional shear flows bounded by quiescent fluid or a uniform stream, such as plane jets, plane mixing layers, plane wakes, and boundary layers.⁵ Only the boundary conditions differ between these flows, which are all characterized by a characteristic flow width $\delta = \delta(x)$. Except near walls, the viscous term is negligible.

As usual in turbulence, this system of equations is not closed since there are three equations for six unknowns, U , V , \bar{p} , σ_{uv} , σ_u , and σ_v . The scale-relativity approach to turbulence^{10–13,16} allows to solve this closure problem by deriving a new expression for the Navier–Stokes equations under turbulent conditions.

B. Schrödinger equation in velocity-space

The fundamental equation of dynamics can be integrated in the scale-relativity paradigm under the form of a Schrödinger equation, in which the constant is no longer the microscopic Planck constant, \hbar , but a new macroscopic constant emerging from self-organization of the system under consideration. Apart from this change of constant, the theory shares the same mathematical structure as standard quantum mechanics, in particular the existence of a wave function that is a solution of the Schrödinger equation and whose modulus squared yields the probability density of states.

The conditions that underlie such a transformation are non-differentiability and fractality, which involve an explicit scale dependence of the various variables. We have shown¹³ that these conditions (infinite number of virtual trajectories, fractal dimension two of each trajectory, and two-valuedness of the derivatives as a consequence of non-differentiability) are satisfied in velocity-space for a turbulent fluid, the fractal dimension two being a manifestation of the K41 scaling $\delta v^2 \sim \delta t$.

This method has been recently applied to turbulent round jets¹⁰ and has allowed us to solve the closure problem in this case. The question raised in the present paper is whether we can obtain a similar result in other types of shear flow, such as flat plate boundary layers, channels, and pipes.

Let us summarize our method (see Refs. 10 and 13 for more details). The time derivative of the NS equations in Newtonian form is given by $da/dt = -\nabla \cdot \dot{p}$. In order to account for the various geometric effects of non-differentiability and fractality, one replaces d/dt by a new total derivative operator:

$$\hat{d} / dt = \partial / \partial t + \mathcal{A} \cdot \nabla_v - i \mathcal{D}_v \Delta_v, \tag{6}$$

where the acceleration \mathcal{A} is now complex as a manifestation of the fundamental two-valuedness of derivatives implied by non-differentiability. One obtains a new form of the equation of dynamics in v -space:

$$\hat{d} / dt \mathcal{A} = \left(\frac{\partial}{\partial t} + \mathcal{A} \cdot \nabla_v - i \mathcal{D}_v \Delta_v \right) \mathcal{A} = \dot{F}, \tag{7}$$

where F contains the pressure gradient term and possibly any applied external force. We introduce a wave function $\psi_v = e^{i\mathcal{S}_v/\hbar_v}$, where \mathcal{S} is the complex action and \hbar_v the new Planck-like constant in v -space, which is proportional to the rate ε of transferred energy dissipated at viscous scales. One can prove^{13,17–19} that Eq. (7) can be integrated under the form of a macroscopic Schrödinger equation in v -space:

$$\mathcal{D}_v^2 \Delta \psi_v + i \mathcal{D}_v \frac{\partial}{\partial t} \psi_v - \frac{1}{2} \phi_v \psi_v = 0 \tag{8}$$

(with $\mathcal{D}_v = \hbar_v/2$), which yields the PDF of velocities as $P_v = |\psi_v|^2$. In this Schrödinger equation, the potential energy takes the universal form of a harmonic oscillator v -potential,^{10,16} which can be written as follows when the mean pressure is time-independent:

$$\phi_v(u, v) = \frac{1}{2} \left(\frac{\partial^2 \bar{p}}{\partial x^2} u^2 + 2 \frac{\partial^2 \bar{p}}{\partial x \partial y} u v + \frac{\partial^2 \bar{p}}{\partial y^2} v^2 \right). \tag{9}$$

III. THEORETICAL ELEMENTS

We shall recall in this section some well-known basic theoretical results concerning the turbulent boundary layer that will be necessary for our theoretical prediction of the Reynolds stress profiles and of the coefficient of correlation of velocities.

A. Thickness of the turbulent boundary layer

It has been shown by Landau and Lifchitz¹⁴ that, $c(x)$ being the solution of the equation

$$c \ln (c R_x)^2 = 2\kappa^2, \tag{10}$$

the thickness of the flat plate turbulent boundary layer (FPTBL) is given by

$$\delta(x) = a_0 x \sqrt{c(x)}. \tag{11}$$

The parameter a_0 is an empirical numerical constant that has not been theoretically predicted to date, for which Landau has given the approximate value $a_0 \approx 0.3$. In this expression, $R_x = Ux/\nu$ is the x Reynolds number. For $\kappa = 0.4$, one finds that a very good approximation for the solution of this equation is

$$c(x) = 0.191 R_x^{-2/7}. \tag{12}$$

This leads to a FPTBL thickness of

$$\delta(x) = \delta_0 x R_x^{-1/7}, \tag{13}$$

where $\delta_0 = \sqrt{0.191} a_0 = 0.437 a_0$. This result demonstrates theoretically the $R_x^{-1/7}$ behavior of the BL thickness, with an exponent slightly different from the original Prandtl value $-1/5$ (see Ref. 20, p. 638).

The numerical constant in this relation is $\delta_0 = 0.16$, which would yield $a_0 = 0.37$, of the order of magnitude of the Landau value.

The wall-friction velocity $v_* = \sqrt{\sigma/\rho}$ is given by $v_* = U\sqrt{c/2}$,¹⁴ i.e.,

$$v_* = 0.309 U R_x^{-1/7}, \quad (14)$$

where σ is the frictional force acting on the unit area of the wall and ρ is the fluid density. Actually, the effect of the $x^{-1/7}$ variation is negligible, and we shall take in what follows $\delta(x) = \alpha_B x$, with $\alpha_B = 0.16 R_x^{-1/7} = (0.06, 0.05, 0.04, 0.03, 0.02)$ for $R_x = (1000, 3000, 15\,000, 100\,000, 2 \times 10^6)$. This can be compared to a turbulent jet whose half-width is αx , with $\alpha \approx 0.2$.

B. Log-law of the wall and Karman constant

The turbulent boundary layer is known to be a two-scale process. This is usually described by using two different normalizations for the distance y along the direction normal to the wall. Far from the wall the flow no longer depends on the viscosity, so that one can use as reference the boundary layer thickness $\delta(x)$, using the dimensionless variable $\eta = y/\delta$. Near the wall, the viscosity matters and one defines $y^+ = yv_*/\nu$, where ν is the molecular viscosity coefficient. Four regions can then be characterized:

- (1) $y^+ = (0 - 5)$, $\eta \approx (0 - 0.0005)$; viscous sublayer; $U = v_* y^+$;
- (2) $y^+ = (5 - 30)$, $\eta \approx (0.0005 - 0.003)$; buffer layer;
- (3) $y^+ = (30 - 1000)$, $\eta \approx (0.003 - 0.1)$; log-law layer; $U = v_*(\kappa^{-1} \ln y^+ + B)$, where $\kappa \approx 0.4$ and $B \approx 5$; and
- (4) $y^+ = (1000 - 10000)$, $\eta \approx (0.1 - 1)$; outer layer; Coles's wake function correction.

The limit of the viscous sublayer is $y^+ = 2/\kappa = 5$. The point where the linear law and the log-law match is given by $y^+ = B + 6 \approx 11$, yielding the estimate $y^+ = 30$ for the end of the buffer layer.

The log-law profile has been theoretically derived from physics principles.^{1,2,14} It is *a priori* valid up to $\eta \approx 0.1$ but remains an excellent approximation in most cases in an overlap layer up to $\eta \approx 0.3$. The empirical parameter κ is the Karman constant, for which we suggest here a theoretical prediction yielding $\kappa = (\sigma_v/\sigma_u)^3 \approx 0.4$, in agreement with its experimentally measured values.

Finally, near the edge of the turbulent region, the log-law must be corrected in the case of plane boundary layers. The correction takes the form of Coles's wake law,²¹ $2(\Pi/\kappa) \sin^2(\frac{\pi\eta}{2\delta})$, with a coefficient Π that vanishes for channels and pipes.

C. Reynolds shear stress: Theoretical profile

It is well known that the Reynolds shear stress, σ_{uv} , in the boundary layer is almost constant for small η values and given by $\sigma_{uv} = v_*^2$ (Ref. 4). For larger values of η , a rough approximation of its profile is given by $\sigma_{uv} = v_*^2(1 - \eta)$. A better solution is obtained by integrating the RANS and continuity equations in the wall normal direction with the assumption that $V = 0$ at the wall:²²

$$\sigma_{uv} = v_*^2 + y \partial_x(p_0(x) - \sigma_v^2) - U \int \partial_x U dy + 2 \int U \partial_x U dy. \quad (15)$$

The term $\partial_x p_0 = -v_*^2/\delta$ yields the standard solution $\sigma_{uv} = v_*^2(1 - \eta)$.⁴ The terms involving the Reynolds stresses are found to be small.

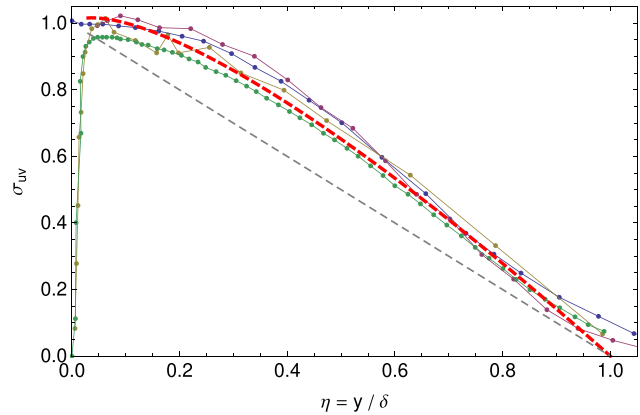


FIG. 1. Comparison between the theoretical prediction from RANS and continuity equations of the Reynolds shear stress in the FPTBL [Eq. (17), red dashed curve] and some of its experimental measurements. Green points and curve: Volino and Schultz;²² blue: Brennen;²³ Magenta: Erm and Joubert,²⁴ brown: Brzek et al.²⁵ The gray dashed line is the standard approximate solution $\sigma_{uv} = 1 - \eta$ (normalized to $v_* = 1$).

The main correction therefore comes from the streamwise velocity U . It is given by the log-law, which remains valid up to $\eta \approx 0.3$:¹⁴

$$U = v_* \left(\frac{1}{\kappa} \ln \eta + B \right). \quad (16)$$

One finally finds that

$$\sigma_{uv} = v_*^2 \left[1 - \eta \left(1 + \frac{\alpha_B}{\kappa^2} (\ln \eta + B\kappa - 2) \right) \right]. \quad (17)$$

It is noticeable that, with the empirical numerical values $\kappa = 0.4$ and $B = 5$, the constant $(B\kappa - 2)$ vanishes. The effect of the Coles's correction of the Reynolds shear stress profile in the outer layer is found to be negligible. This theoretical expectation is in good agreement with the experimental measurements, as exemplified in Fig. 1.

IV. THEORETICAL PREDICTION OF THE RATIO OF REYNOLDS STRESSES

Tennekes and Lumley⁴ have argued that the energy in the u component differs from that in the v component because the major production term feeds energy into σ_u^2 (along the axial direction), so the energy must leak into σ_v^2 (along the radial direction) by inertial interaction. Since the two effects (axial supply and radial leakage) are determined by the same turbulence dynamics, they concluded that $K = (\sigma_u^2 - \sigma_v^2)/(\sigma_u^2 + \sigma_v^2) \approx \text{cst}$ and that it should be less than unity. This implies that $R = \sigma_u/\sigma_v > 1$ should be close to a constant.

We have derived in Ref. 10 the theoretically expected possible values of R by only using a self-evident property of the turbulent jet that appears clearly in this analysis and in the governing equations: the mere fact that $K \geq 0$, i.e., $\sigma_u \geq \sigma_v$. Let us briefly recall here the argument.

We apply this inequality in the scale-relativity framework, where the derivative of the Navier–Stokes equations takes a (macroscopic) quantum-like Schrödinger form. We have decomposed the global Gaussian turbulent velocity fluctuations variances σ_u^2 and σ_v^2 in terms

of two-dimensional quantized harmonic oscillators (QHOs), which are known to be defined by quantum numbers $\{n_u, n_v\}$.

The above inequality, applied on the various excited states of a 2D QHO, simply becomes $n_u \geq n_v$. At this level of the analysis, we take $R = \text{cst}$, in agreement with Tennekes and Lumley's argument.

Our first derivation of the range of possible values for R has been obtained in the framework of the study of turbulent jets. This has allowed us to consider only the uncorrelated turbulent velocities on the centerline of the jet. This is no longer possible in the BL case where the correlation coefficient may be everywhere different from zero (and equal to ≈ 0.4 : this is another puzzle for which we suggest a solution here). However, one can show that the velocity correlation has a very small effect on the ratio R in the BL case. Therefore, we can write

$$\sigma_{n_u}^2 = (2n_u + 1) \sigma_{uF}^2, \quad \sigma_{n_v}^2 = (2n_v + 1) \sigma_{vF}^2, \quad (18)$$

where σ_{uF}^2 and σ_{vF}^2 are the variances of the normal (ground) state for the u and v coordinates (the PDFs of which are Gaussian).

In the scale-relativity approach, turbulence and its main effects such as intermittency come from the emergence of a new acceleration component, which can be written as $A_q = \pm \mathcal{D}_v(\partial_v P_v)/P_v$.¹³ The probability density P_v of QHO excited states is zero, $P(v_i) = 0$, for some values of the velocity v_i , which implies the divergence of this acceleration. We have shown that this result explains and accounts in detail for many features of turbulence (e.g., large tails of acceleration PDF, structure functions).¹³

The ground state, for its part, has no such zeros. We have therefore interpreted its manifestation as corresponding to the transition between laminar and turbulent flow, which occurs around the edge of the turbulent region. This means that, when approaching the edge of the boundary layer, the turbulent fluctuations become that of the ground state, $\sigma_u = \sigma_{uF}$ and $\sigma_v = \sigma_{vF}$. In this regime, we expect isotropy of the fluctuations, so $\sigma_{uF} \rightarrow \sigma_{vF}$ and therefore $R_F = \sigma_{uF}/\sigma_{vF} \rightarrow 1$ and $R \rightarrow 1$. Experimental data fairly support this expectation, since the turbulent intensities are found to become equal when approaching the boundary layer edge, for $\eta = 0.8$, and R to finally falls down to $R = 1$ at $\eta \approx 0.9 - 1$, as can be seen in Figs. 3 and 16.

The global variances will therefore be $\sigma_u^2 = \langle \sigma_{ui}^2 \rangle$ and $\sigma_v^2 = \langle \sigma_{vi}^2 \rangle$, where the mean is taken on all the QHOs with fluctuating quantum numbers. We find, finally, that

$$R^2 = \frac{\sigma_u^2}{\sigma_v^2} = \frac{\langle 2n_u + 1 \rangle}{\langle 2n_v + 1 \rangle} R_F^2 \quad (19)$$

for the PDF of n_u given by the Gibbs distribution and $n_v = \{0, 1, 2, \dots, n_u\}$.

When the Reynolds number is large enough, this distribution is almost flat (as a first approximation) and we can take the direct average.

Let us first consider some selected given value of n_u . From statistical physics, one expects only small quantum numbers to play a leading role. For $n_u = 2$, $\langle n_v \rangle = 1$, then when $R_F = 1$ (toward the BL edge), $R = \sqrt{5/3} = 1.29$; for $n_u = 3$, $R = \sqrt{7/4} = 1.32$; for $n_u = 4$, $R = \sqrt{9/5} = 1.34$.

More generally, taking all the values of n_u between 1 and $(n_u)_{\text{max}}$, we find the R values given in Fig. 2. Identifying the resulting interval $(1.29 - 1.41)$ with $\pm 2 \sigma$, we obtain

$$R_{\text{th}} = 1.35 \pm 0.03. \quad (20)$$

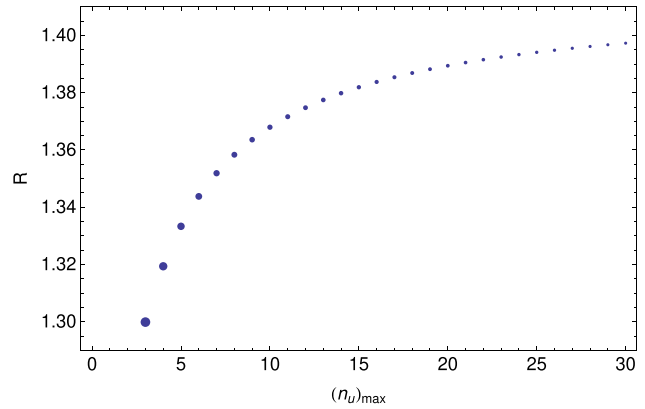


FIG. 2. Expected distribution of values for the ratio $R = \sigma_u/\sigma_v$, when the ground state ratio $R_F = 1$. It is derived from the decomposition of the turbulent fluctuation velocities into QHOs, for a maximum quantum number $n_u = 30$. The density of points increases for higher R values toward ~ 1.41 , but the probability of smaller values toward ~ 1.3 (represented by the point size) is larger according to the Gibbs distribution. This yields an average $\langle R \rangle \approx 1.35$.

This theoretical prediction is in satisfactory agreement with the results of laboratory and numerical experiments in the relevant region (far from the wall) for flat boundary layers, channels, and pipes (see Figs. 3, 4, and 16).

This result is still reinforced by accounting for the expected Gibbs distribution of the QHOs, which favor smaller values of the quantum numbers. The probability for a QHO to be in a given state of quantum number n can be written as follows:³⁰

$$w(n) = e^{-\frac{1}{2}(2n+1)\frac{\hbar_v \omega}{T_v}}, \quad (21)$$

where $T_v = k_B a^2$ is the equivalent of temperature in v -space, $\hbar_v = \varepsilon = \sigma_v^3/L$, $\omega = 2\pi/T$. We have found from Mordant data that $T = NT_L$, with $N \approx 6$, so $\omega \approx 1/T_L$. We can now relate all these

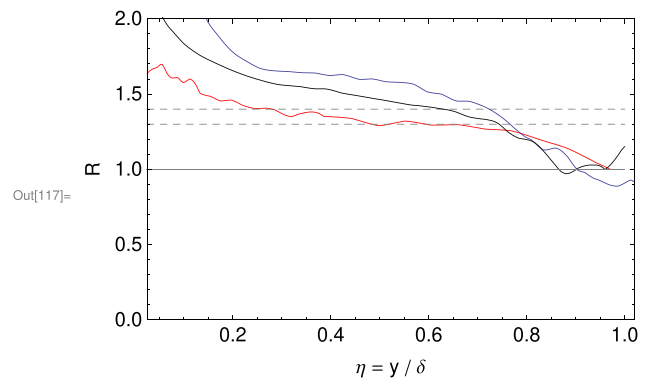


FIG. 3. Experimental profiles of the ratio of turbulent intensities $R = \sigma_u/\sigma_v$, across the turbulent region in the direction normal to the plane. The red curve results from data provided by Shafi and Antonia,²⁶ the black curve from Brenner,²³ and the blue curve from DNS by Spalart.^{27,28} We have shown as horizontal dashed lines the interval $R = (1.3 - 1.4)$ expected when the ground state ratio $R_F \rightarrow 1$ (approaching the BL edge) and as continuous gray line the value $R = 1$ expected on the edge.

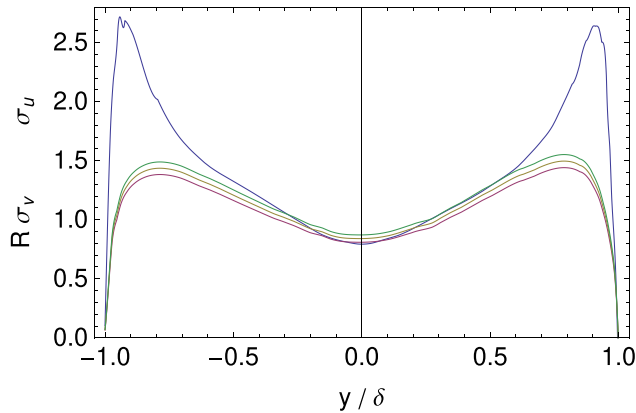


FIG. 4. Comparison between the streamwise turbulent intensity profile $\sigma_u(\eta)$ in a channel (blue curve) and the scaled normal turbulent intensity $R\sigma_v(\eta)$, for three values of $R = (1.30, 1.35, 1.40)$ (magenta, brown, and green curves), from the DNS data of Kim *et al.*²⁹ This supports our theoretical expectation according to which $\sigma_u \approx 1.35\sigma_v$ in the central region of the channel, far from the walls (which lie at $\eta = \pm 1$).

constants to $R_\lambda = \sqrt{15L\sigma_v/\nu}$, since $\sigma_v \sim R_\lambda^2$, $\sigma_a^2 \sim R_\lambda^3$, and $T_L \sim R_\lambda^{-2}$. One finally finds

$$\frac{\hbar_v \omega}{T_v} = \frac{\sqrt{15} \pi C_0}{k_B A_0 N R_\lambda}, \tag{22}$$

where C_0 and A_0 are the two Kolmogorov constants (having values $\approx 4 - 6$), $C_0 = 2\sigma_v^2/\varepsilon T_L$ and $A_0 = \sigma_a^2 \tau_\eta/\varepsilon$. Finally, we find that the constant in the Gibbs distribution is proportional to $1/R_\lambda$. This means, as could be expected, that higher quantum numbers n contribute more for higher Reynolds numbers. Finally, the probability can be written as

$$w(n) = \exp\left[-\frac{R_{\lambda_0}}{R_\lambda} \left(n + \frac{1}{2}\right)\right], \tag{23}$$

where the constant $R_{\lambda_0} \approx 100$ from an analysis of Mordant's data.

With this value we find, for fully developed turbulence with reduced Reynolds number $R_\lambda = 1000$ (i.e., $Re \approx 70\,000$) and maximum quantum numbers, respectively, $n_{max} = (10, 20, 30)$, mean values of the R ratio $\langle R \rangle = (1.31, 1.33, 1.335)$. For larger values, $n_{max} \leq 50$, the mean value of R stabilizes at $\langle R \rangle = 1.34$.

V. POSSIBLE SOLUTION TO THE KARMAN CONSTANT PROBLEM

It has been argued by Landau and Lifchitz¹⁴ that in the flat plate boundary layer, the flow is characterized by no constant parameter of length that would allow to determine the scale of the turbulent flow. In consequence, he concludes that the main scale of turbulence is determined by the distance itself, i.e., the only available natural scale in the infinite flat plate problem is the height y . Therefore,

$$L_x = y. \tag{24}$$

This theoretical expectation is supported by Tennekes and Lumley analysis of the link between Reynolds stress and vortex stretching.⁴ They argue that the existence of a Reynolds stress requires that the velocity fluctuations u and v be correlated. The eddies are continuously

losing energy to smaller eddies, so they need shear to maintain their energy: the most powerful eddies thus are those that can absorb energy from the shear flow more effectively than others. They conclude, in agreement with Townsend³¹ and Bakewell and Lumley,³² that the eddies that are most effective in both maintaining the u, v correlation and in extracting energy from the mean flow are vortices whose principal axis is roughly aligned with that of the mean strain rate. These three dimensional vortices with vorticity ω are stretched by the rate of strain S with ω parallel to S along a direction making an angle of $\approx 45^\circ$ with the flat plate (see their Fig. 2.5 and p. 41).

Experimental observations of these eddies clearly support this expected angle of 45° (see, e.g., Refs. 33 and 34) and therefore the evidence for the fact that the fundamental length scale is $L_x = y$.

In the scale-relativity approach to turbulence, the fundamental constant \hbar_V in velocity-space is identical (or at least proportional) to the K41 rate of transferred energy ε . This implies the following relation:

$$\hbar_V = \frac{\sigma_u^3}{L_x} = \frac{\sigma_v^3}{L_y}, \tag{25}$$

which relates the anisotropy of the velocity turbulent fluctuations with the space anisotropy. Therefore,

$$\frac{L_y}{L_x} = \frac{\sigma_v^3}{\sigma_u^3} = \frac{1}{R^3}. \tag{26}$$

Finally, the length scale along the transverse direction is, therefore,

$$L_y = \frac{y}{R^3}. \tag{27}$$

The mean streamwise velocity is solution of the differential equation

$$\frac{dU}{dy} = \frac{v_*}{L_y} = \frac{R^3 v_*}{y}, \tag{28}$$

which is integrated under the form of the well-known log-law of the mean velocity profile given by

$$U = \frac{v_*}{\kappa} \ln \frac{y}{y_0}, \tag{29}$$

in which κ is the Karman constant for which we have therefore obtained the following theoretical prediction:

$$\kappa = \frac{1}{R^3}. \tag{30}$$

From the previously theoretically estimated range for $R = \sigma_u/\sigma_v = 1.35 \pm 0.03$, we can now derive the possible values of the Karman constant:

$$\kappa = 0.405 \pm 0.025, \tag{31}$$

which is in good agreement with its measured values.

Actually, statistical analysis of the available data⁶ shows that the differences between the three canonical flows could be much larger than the uncertainty in the extracted overlap parameters. This suggests that the von Karman coefficient may not be strictly universal and exhibits a small dependence on the flow geometry.

The mean value of κ has been found to be 0.37, 0.39, and 0.41, respectively, for channels, flat plate boundary layers, and pipes.⁶

These values correspond to, respectively, $R = 1.39, 1.37,$ and 1.35 for $R_F = 1$, which clearly lie in the range expected from the present v -Schrödinger/QHO approach.

More generally, Nagib and Chauhan⁶ have found a full range of measured values, $\kappa = 0.35 - 0.45$. Smart⁹ has reported the existence of atmospheric measurements showing κ values as low as 0.35 ³⁵ and as high as 0.46 ³⁶ and of direct numerical simulation of boundary layer turbulence revealing κ values that can range from 0.384 ± 0.004 ³⁷ to 0.452 .³⁸

The full range of observed κ values, $0.35 - 0.46$, thus exactly corresponds to just the full range of possible R values (for $R_F = 1$), which lie between $R_{\max} = \sqrt{2} = 1.414$ yielding $\kappa = 2^{-3/2} = 0.35$ and $R_{\min} = \sqrt{5/3} = 1.29$ yielding $\kappa = (3/5)^{3/2} = 0.46$.

VI. SOLUTION FOR THE REYNOLDS STRESS PROFILE IN THE NORMAL DIRECTION

Neglecting small terms, the RANS equation for the boundary layer yields the following general result:^{4,5}

$$p = p_0(x) - \sigma_v^2. \tag{32}$$

Therefore, the pressure in the potential of the v -Schrödinger equation can be replaced by the opposite of the Reynolds normal stress. We denote by R_F the ratio of turbulent intensities in the ground state and by G_v the ratio of the velocity fluctuation variance over that of the ground state:

$$R_F = \frac{\sigma_{uF}}{\sigma_{vF}}, \quad G_v = \frac{\sigma_v^2}{\sigma_{vF}^2}. \tag{33}$$

For QHOs, $\sigma_v^2 = (2n_v + 1)\sigma_{vF}^2$ in a given excited state of probability $P(n_v)$ such that $\sum P(n_v) = 1$, so $G_v = \sum P(n_v)((2n_v + 1))$, where $P(n_v)$ is given by statistical physics.³⁰

We call ρ_F the coefficient of correlation of velocities in the ground state and L_v the integral length scale in the normal direction. Then, the k_v equation reads¹⁰

$$k_v = -\partial_y \partial_y \sigma_v^2 = H \frac{R_F^2 + \rho_F^2}{R_F^2(1 - \rho_F^2)^2} \sigma_v^2, \tag{34}$$

where

$$H = \frac{G_v^2}{4L_v^2}. \tag{35}$$

One of the main specificities of the turbulent BL with respect to the jet lies in the nature of the integral length scale L_v . As recalled above, it is proportional to the normal distance, $L_v = \kappa y$, the coefficient of proportionality being just the Karman constant we have theoretically predicted above to be $\kappa = 1/R^3 \approx 0.4$.

Therefore, the k_v equation in the FPTBL case becomes

$$y^2 \partial_y \partial_y \sigma_v^2(y) + B_0 \sigma_v^2(y) = 0, \tag{36}$$

where

$$B_0 = \frac{G_v^2}{4\kappa^2} \frac{(1 + \rho_F^2/R_F^2)}{(1 - \rho_F^2)^2}. \tag{37}$$

This equation is doubly scaling, i.e., invariant under scale factors on both y and σ_v . It can then be equivalently written in terms of the

dimensionless normal distance $\eta = y/\delta$. Under the approximation $B_0 \approx \text{cst}$, the solution of this equation reads

$$\sigma_v^2 = A \sqrt{\eta} \sin(a_p \ln \eta), \tag{38}$$

where $a_p = \sqrt{B_0 - 1/4}$. This function shows interesting multi-scale properties reminiscent of the two-scale nature of the flat plate boundary layer^{4,5,14} (see Appendix A).

It presents a peak at a distance η_p , in terms of which the coefficient a_p can be written to a good approximation as $a_p = -0.78313 + 8.108 \eta_p - 9.295 \eta_p^2$, valid for η_p in the range $(0.17 - 0.25)$. An improved expression for a_p is given in Appendix A.

As can be seen in Fig. 5, this theoretical prediction is in good agreement with the results of laboratory and numerical experiments for $\eta_p \approx 0.15 - 0.20$ in turbulent plane boundary layers. In the case of channels and pipes, the edge of the boundary layer $\eta = 1$ for $y = \delta(x)$ is replaced by the center plane of a channel of width $2h$ at $\delta = h$ and the centerline of a pipe of radius r at $\delta = r$. As expected, the behavior of the various functions near $\eta = 1$ becomes different from the free case. We show in Fig. 6 that our theoretical prediction remains nevertheless in good agreement with experiments up to $\eta \approx 0.7$.

Introducing the turbulent intensity amplitude μ_B (unknown at this stage) and the (known) wall-friction velocity v_* , the full solution reads

$$\sigma_v^2 = \mu_B^2 v_*^2 \sqrt{\frac{\eta}{\eta_p}} \frac{\sin(a_p \ln \eta)}{\sin(a_p \ln \eta_p)}. \tag{39}$$

The situation is therefore comparable to the turbulent round jet case¹⁰ where we have found in the central region of the jet $\sigma_v^2 = \mu^2 U_C^2 \cos(\sqrt{3}\eta/\alpha)$, where $\eta = r/x$ and U_C is the mean axial velocity on the jet centerline. In both cases, we have derived from the k_v equation a generic Reynolds stress profile, while the full solution depends also on a numerical amplitude factor (μ_B and μ) and on another numerical factor characterizing the profile shape (η_p and α). These numerical factors can be theoretically derived from other equations, as we shall now see.

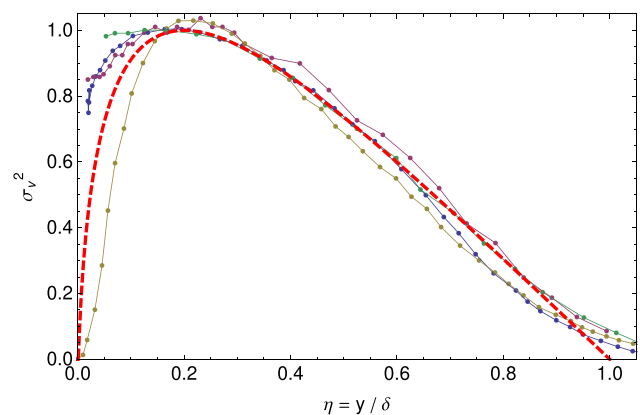


FIG. 5. Comparison between our theoretical prediction of the Reynolds stress pure profile σ_v^2/μ_B^2 in a flat plate turbulent boundary layer (red dashed curve, $\eta_p = 0.2$), with some examples of its experimental and DNS measurements. Blue points and curve: Brennen;²³ magenta: Shafi and Antonia;²⁶ beige: DNS by Spalart;²⁷ green: Ern and Joubert.²⁴

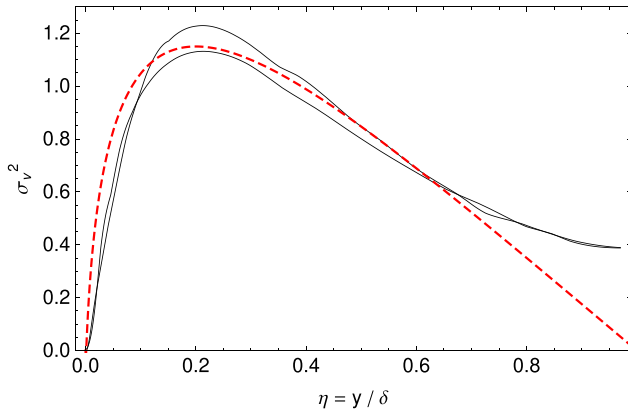


FIG. 6. Comparison between our theoretical prediction of the Reynolds stress profile σ_v^2 in a turbulent boundary layer (red dashed curve, $\eta_P = 0.2$), with the result for a channel from DNS by Kim *et al.*²⁹ The two black curves correspond to the up and down parts of the channel. The walls lie at $\eta = 0$ and the centerplane at $\eta = 1$.

VII. THEORETICAL PREDICTION OF THE TURBULENT INTENSITY AMPLITUDE

We have found above that the k_v equation yields a solution for the pure turbulent intensity profile that agrees with experimental measurements. However, at this level of the analysis, its amplitude remains unknown. As we shall now see, the amplitude μ_B can be obtained from the other equations derived from the QHO v -Schrödinger equation. The method is the same as that used for turbulent jets,¹⁰ but now it is applied to the boundary layer.

A. Decorrelation of velocities for QHOs

A direct approach for obtaining a theoretical solution for the values of μ_B consists of fully solving the equations for the excited states. This can be done by performing a rotation by an angle θ to a coordinate system $(\mathcal{U}, \mathcal{V})$ where the turbulent velocities become decorrelated. One finds this decorrelation angle to be given by

$$\tan(2\theta) = \frac{2k_{uv}}{k_v - k_u} = \frac{2\sigma_{uv}}{\sigma_u^2 - \sigma_v^2}. \quad (40)$$

Setting $T = \tan(2\theta)$ and $A = 1/\sqrt{1+T^2}$, one obtains

$$C = \cos\theta = \sqrt{\frac{1+A}{2}}, \quad S = \sin\theta = \sqrt{\frac{1-A}{2}}. \quad (41)$$

The new coefficients $k_{\mathcal{U}}$ and $k_{\mathcal{V}}$ in the QHO potential read

$$k_{\mathcal{U}} = k_u C^2 - 2k_{uv}CS + k_v S^2, \quad k_{\mathcal{V}} = k_v C^2 + 2k_{uv}CS + k_u S^2. \quad (42)$$

Since $k_{\mathcal{U}\mathcal{V}} = 0$, the two variables are now separated and the expressions of the Reynolds stresses are easily derived from the standard QHO relations:

$$\sigma_{\mathcal{U}}^2 = \frac{(2n_u + 1)\hbar_{\mathcal{V}}}{2\sqrt{k_{\mathcal{U}}}}, \quad \sigma_{\mathcal{V}}^2 = \frac{(2n_v + 1)\hbar_{\mathcal{U}}}{2\sqrt{k_{\mathcal{V}}}}. \quad (43)$$

Finally, we obtain the expressions for the three Reynolds stresses in the initial coordinate system:

$$\sigma_u^2 = C^2\sigma_{\mathcal{U}}^2 + S^2\sigma_{\mathcal{V}}^2, \quad \sigma_v^2 = S^2\sigma_{\mathcal{U}}^2 + C^2\sigma_{\mathcal{V}}^2, \quad \sigma_{uv} = CS(\sigma_{\mathcal{U}}^2 - \sigma_{\mathcal{V}}^2). \quad (44)$$

B. Equation for the amplitude

This system cannot be directly used because of the problem encountered with the k_u equation. In the absence of a source term (until now unknown), it corresponds to a repulsive harmonic oscillator, which seems to contradict the laboratory results and those obtained from numerical experiments.

A solution to this problem consists of using the relation $\sigma_u = R\sigma_v$ and the fact that σ_{uv} is known in order to calculate k_u , instead of using its direct expression $k_u = -\partial_x \partial_x \sigma_v^2$. One obtains

$$k_u = k_v - k_{uv} \frac{\sigma_v^2}{\sigma_{uv}} (R^2 - 1). \quad (45)$$

Applying this method to the pure normalized profiles (denoted by the subscript o), this yields the following new expressions:

$$k_{uo} = k_{vo} - k_{uvo} (R^2 - 1) \mu^2 \frac{\sigma_{vo}^2}{\sigma_{uvo}}, \quad T = \frac{2\sigma_{uvo}}{\mu^2 (R^2 - 1) \sigma_{vo}^2}, \quad (46)$$

$$k_{\mathcal{U}o} = k_{vo} - k_{uvo} C \left(\frac{\mu^2 (R^2 - 1) \sigma_{vo}^2}{\sigma_{uvo}} C + 2S \right), \quad (47)$$

$$k_{\mathcal{V}o} = k_{vo} - k_{uvo} S \left(\frac{\mu^2 (R^2 - 1) \sigma_{vo}^2}{\sigma_{uvo}} S + 2C \right). \quad (48)$$

As previously seen, the generalized macroscopic Planck constant reads

$$\hbar_{\mathcal{V}} = \frac{\sigma_v^3}{L_{v0}}, \quad (49)$$

where the length scale must be proportional to y : $L_{v0} = \kappa_0 y$. It depends almost linearly on the axial distance since $y = \delta \eta = \alpha_B x \eta$. We have shown in Sec. III A that $\alpha_B = \delta_0 R_x^{-1/7}$, then it depends slightly on x as $x^{-1/7}$. We find that this dependence can be neglected, so we only describe the Reynolds number dependence considering various values of α_B in the range $(0.03 - 0.06)$ corresponding to $R_x = (10^5 - 10^3)$.

We finally obtain an implicit equation for the turbulent intensity amplitude μ_B ,

$$Q = 2\kappa_0 \alpha_B \eta x \frac{\sigma_{uvo}}{\mu_B^2 \sigma_{vo}^3} \sqrt{1 + \frac{1}{T^2}} \left[\left(n_u + \frac{1}{2} \right) \frac{1}{\sqrt{k_{\mathcal{U}o}}} - \left(n_v + \frac{1}{2} \right) \frac{1}{\sqrt{k_{\mathcal{V}o}}} \right]^{-1} = 1. \quad (50)$$

This equation can be theoretically solved on the basis of our previously acquired knowledge of the pure profile $\sigma_{vo}^2(\eta)$ and of the Reynolds shear stress σ_{uvo} . It therefore depends on the quantum numbers n_u and n_v , on the parameters η_P , R , α_B , and μ_B , and on the scaled radial distance $\eta = r/x$. It is solved by the values of η_P , R , α_B , and μ_B , which ensure a constant radial profile $Q(\eta) = \text{cst}$, provided they exist, and is expected to yield a relation $\mu_B = \mu_B(\eta_P, R, \alpha_B)$. The value of κ_0 can be subsequently derived from the equation $Q = 1$.

As recalled above, statistical physics implies that the states with the smallest quantum numbers are the most probable. However, we have also seen that, in our framework, the ground state $n_u = n_v = 0$ cannot correspond to a fully turbulent state. This is due to the fact that

it is devoid of velocity values for which $P_v(v_i) = |\psi_v|^2(v_i) = 0$, while we have identified the zeros of the velocity PDF and the supplementary acceleration component they involve as the source of the main turbulent characteristics.^{12,13} Therefore, the ground state is considered to apply only in the turbulent–laminar transition, at the interface between the two regimes.

As a consequence, the most probable state is given by the quantum numbers $n_u = 2$, $n_v = 1$, the other states contributing only in a minor way. We have therefore specifically applied the above equation $Q = \text{cst}$ to this case.

Regarding the Reynolds normal stress pure profile, we have used our theoretical solution normalized to one at maximum,

$$\sigma_{vo}^2 = \sqrt{\frac{\eta}{\eta_P}} \frac{\sin(a_P \ln \eta)}{\sin(a_P \ln \eta_P)}, \quad (51)$$

where we recall that $a_P = -0.78313 + 8.108 \eta_P - 9.295 \eta_P^2$.

As for the Reynolds shear stress, we have used the solution of the RANS and continuity equations given by Eq. (17), which can be written as follows to a good approximation:

$$\sigma_{uv} = v_*^2 \left(1 - \eta - \frac{\alpha_B}{\kappa^2} \eta \ln \eta \right). \quad (52)$$

We have also considered the usual approximative solution,⁴ $\sigma_{uvo} = 1 - \eta$, and a polynomial fit of the Reynolds shear stress measurement by Erm and Joubert,²³ which can be written as $\sigma_{uv} = 0.9838 + 0.478\eta - 2.294\eta^2 + 0.872\eta^4$. As we shall see, they yield solutions that frame the more exact solution and are compatible with it.

C. Numerical solution by optimization and fit

We have calculated $Q(R, \mu_B, \alpha_B, \eta_P, \kappa)$ for a large range of parameter values, $R = (1.2 - 1.6)$, $\mu_B = (0.8 - 1.6)$, $\alpha_B = (0.03 - 0.06)$, $\eta_P = (0 - 0.4)$, and $\kappa = (0.37 - 0.43)$.

Examples of Q profiles obtained are given in Fig. 7, which demonstrates the existence of very precise solutions for the equation $Q = 1$. The residual standard deviation, σ_Q , with respect to a flat profile

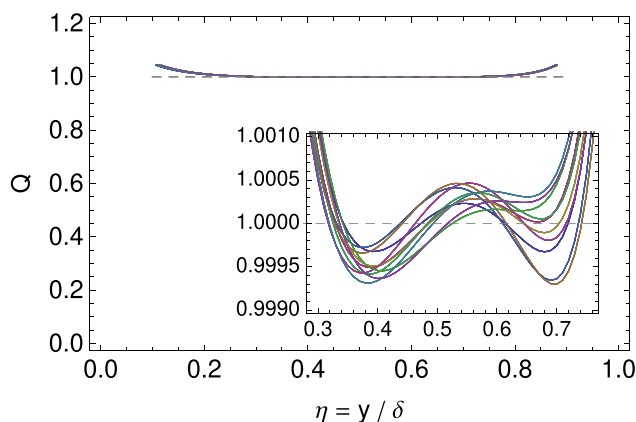


FIG. 7. Examples of Q profiles demonstrating that there exists values of the parameters $(R, \alpha_B, \eta_P, \mu_B)$ for which $Q \approx 1$ in a large interval $\eta \approx (0.2 - 0.8)$. The standard deviations for these solutions on the range $(0.3 - 0.75)$ is $\sigma_Q < 0.0003$. The inset is a zoom by a factor ≈ 300 showing the detailed profiles of these solutions.

$Q(\eta) = 1$ has been calculated for each set of parameters in the range $\eta = 0.3 - 0.75$. The smallest values of this dispersion reach $\sigma_Q < 0.0002$.

In a run taking $\kappa = 0.4$, a fit of the parameter subset such that $\sigma_Q < 0.002$ yields with a high statistical significance (Student's $t > 80$ for the R coefficients and > 35 for the others):

$$\mu_B = 9.692 - 10.70R + 3.14R^2 + 1.64\alpha_B + 4.73\eta_P - 18.54\eta_P^2. \quad (53)$$

The dependence of μ_B on α_B and η_P is weak, yielding only small corrections to the mere function of R (see Fig. 8), which can be written as

$$\mu_B(R) = R_0 - 2.26(R - R_0) + 3.11(R - R_0)^2, \quad (54)$$

where $R_0 = 1.344$ is the value for which $\mu_B = R$. This value is just the central value predicted from the QHO Schrödinger equation (Ref. 10 and Sec. IV). This result is illustrated in Fig. 9, where we have plotted the values of μ_B in function of R for the various parameters that satisfy $\sigma_Q < 0.002$. In this figure, the values of μ_B have been corrected for the small α_B and η_P dependence according to the above fit Eq. (53).

From the predicted values of $R = 1.34 \pm 0.04$, we therefore derive a theoretical prediction for the range of possible μ_B values, $\mu_B = 1.36 \pm 0.09$, leading to the final conclusion that $\mu_B \approx R \approx 1.35$.

We give in Appendix B the results of our numerical calculations and their fit for different choices of the function $\sigma_{uv}(\eta)$. The agreement between the slopes of the linear term in all cases is remarkable. Only the value for which $\mu_B = R$ changes slightly from 1.33 to 1.35 then 1.38, which remains in the theoretically predicted range of $R = \sigma_u / \sigma_v$.

Finally, the value obtained for the constant κ_0 is compatible with $\kappa_0 = 1$, although with a large dispersion (we find $\kappa_0 = 1.04$ with a standard error $\sigma_{\kappa_0} = 0.30$). This means that the length scale entering into the definition of the v -Planck constant is just $L_{v0} = \kappa_0 y \approx y$.

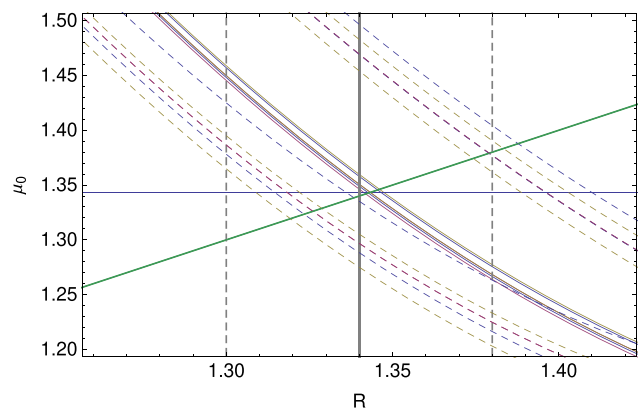


FIG. 8. Relation $\mu_B(R)$ solving the equation $Q = \text{cst}$ [Eq. (50)]. The σ_v profile input in this equation is the theoretical solution of the k_v equation, while σ_{uv} is the solution of the RANS and continuity equations Eq. (52). The different continuous curves correspond to the range of possible values for α_B and η_P . The equality $\mu_B = R$ is reached for $R_0 = 1.344$. The dashed curves correspond to two other choices, the standard simple solution $\sigma_{uv} = 1 - \eta$ and a fit of (EJ)²⁴ data. It is compared to the range of predicted values for R from quantized QHOs, $R = 1.34 \pm 0.04$, yielding possible values for μ_B in the range $(1.28 - 1.45)$.

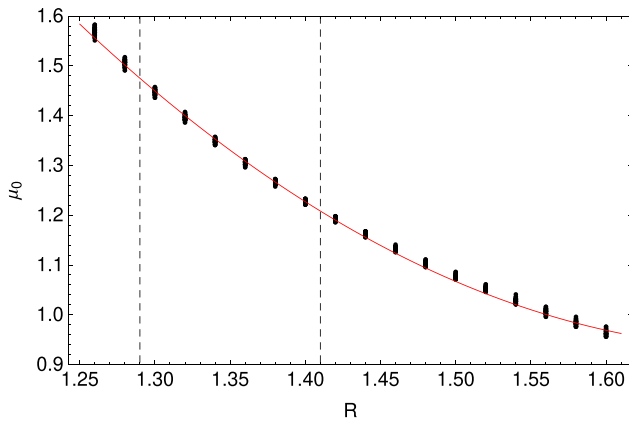


FIG. 9. Values of (R, μ_B) solving the equation $Q = \text{cst}$ [Eq. (50)], where μ_B is corrected for the small dependence on α_B and η_P . The σ_v profile input in this equation is our theoretical solution of the k_v equation Eq. (38), while the σ_{uv} profile is the solution of the RANS and continuity equations Eq. (52). The red continuous curves are the resulting fit yielding the searched relation $\mu_B = \mu_B(R)$, which is the solution of the equation $Q=1$. It is indistinguishable in the relevant range $R \approx (1.29 - 1.41)$ from the series analytic solution given in Eq. (55).

D. Analytical solution by power series expansion

We have obtained an approximate analytical solution for the function $\mu_B(R, \alpha_B, \eta_P, \kappa)$ by performing a power series expansion of Q in function of η and of the various parameters. We set $n = \eta - \eta_0$, $r = R - R_0$, $m = \mu_B - \mu_{B0}$, $a = \alpha_B - \alpha_{B0}$, $p = \eta_P - \eta_{P0}$ and $k = \kappa - \kappa_0$. The resulting expression of $Q = A + Bn + \mathcal{O}[n^2]$ around $(R_0, \mu_{B0}, \alpha_{B0}, \eta_{P0}, \kappa_0) = (1.35, 1.35, 0.045, 0.16, 0.40)$ to first order in n and to second order in the other parameters is given in Appendix C, Eq. (C5).

Then, we express the theoretically predicted constancy of Q by requiring the cancellation of the linear term, $B=0$. This results in the following second order power series expression for $m = \mu_B - 1.35$:

$$m = (-0.0336 + 1.596a - 0.694p - 0.357k - 13.04ak + 1.29k^2 - 14.90ap + 1.83kp) + (-2.161 - 5.079a + 1.297p + 0.421k + 62.82ak - 6.75k^2 + 48.91ap - 9.85kp)r + (4.317 - 39.45a - 2.18p - 6.36k - 177.3ak + 39.7k^2 - 249.5ap + 44.8kp)r^2. \tag{55}$$

This function is plotted in Fig. 10 for various values of the parameters. It is in good agreement with the fit of the optimized numerical results, as it can be seen in Figs. 9 and 23.

E. PDFs of parameters

The equation $Q=1$ provides us with a relation $\mu_B = \mu_B(R, \eta_P, \alpha_B, \kappa)$ and also with PDFs for some of the parameters, and therefore with possible theoretical predictions of their values. Indeed, as we shall see, while we have calculated Q for a uniform distribution of the parameters in large intervals, the values of these parameters which yield $Q = \text{cst}$ with a small standard deviation $\sigma_Q \rightarrow 0$ are no longer uniformly distributed. They show either limits not explained by the limits of the initial range or, in some cases, well-defined narrow peaks of probability, allowing a theoretical prediction of the most

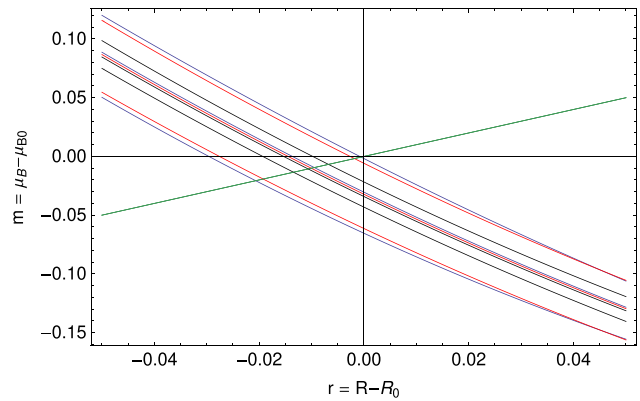


FIG. 10. Plot of the analytical function $m(r)$, where $R = R_0 + r$ and $\mu_B = \mu_{B0} + m$ with $R_0 = \mu_{B0} = 1.35$, derived from the equation $Q = \text{cst}$, for various values of the parameters, as given in Eq. (55). The different curves correspond to $a = (-0.02, 0, 0.02)$, i.e., $\alpha_B = (0.025, 0.045, 0.065)$ (blue curves), $p = (-0.04, 0, 0.04)$, i.e., $\eta_P = (0.12, 0.16, 0.20)$ (red curves), and $k = (-0.03, 0, 0.03)$, i.e., $\kappa = (0.37, 0.40, 0.43)$ (black curves). The central values have been slightly displaced for clarity of the plot. The green line shows the values for which $\mu_B = R$.

probable values of the parameters and of the standard deviation around these probability peaks.

1. PDF of α_B

We have performed a specific numerical run for studying the effect of the parameter $\alpha_B = \delta_0 R_x^{-1/7}$, which defines the BL thickness $\delta(x) = \alpha_B x$. We have taken α_B values in the range $0.002 - 0.24$ (98 290 values of the parameters). The resulting PDF depends of the limit chosen for σ_Q . When $\sigma_Q < 0.01$, one finds a PDF increasing toward small α_B values (large Reynolds numbers) with a peak at $\alpha_B = 0.006$ ($R_x \approx 10^{10}$) and a slower decrease for $\alpha_B > 0.03$ ($R_x < 10^5$). When we take the values of parameters such that $\sigma_Q < 0.003$, one finds a probability peak at $\alpha_B = 0.07$ ($R_x \approx 300$), which is of the order of magnitude of the smallest critical Reynolds number for this kind of flow (see Fig. 11).

Finally, one can ask whether a theoretical prediction is possible for the constant δ_0 . We have therefore directly plotted the PDF of R_x for $\delta_0 = 0.16$, as shown in Fig. 11. We find, as could be expected, a flat distribution for large enough Reynolds numbers, but also a very clear transition around $R_x = 1$, which can be interpreted as a theoretical prediction of our chosen value for δ_0 .

2. PDF of the ratio R of turbulent intensities

The PDF of R is shown in Fig. 12 (left). One finds $1.3 < R < 1.48$ directly from $Q = \text{cst}$ using neither the value $R = \sqrt{5/3} \approx 1.29$ for $n_u = 2$ and $n_v = 1$ nor the mean result from QHOs, $\langle R \rangle \approx 1.35$. The PDF of μ_B is rather flat since it just reflects that of R and its relation in function of R , $\mu_B \approx 1.35 - 2.25(R - 1.35)$.

3. PDF of η_P

In addition, we also find a theoretical prediction for the possible values of η_P , which is such that $\eta_P < 0.24$ with a PDF showing a peak at $\eta_P \approx 0.175$ for $\sigma_Q < 0.007$.

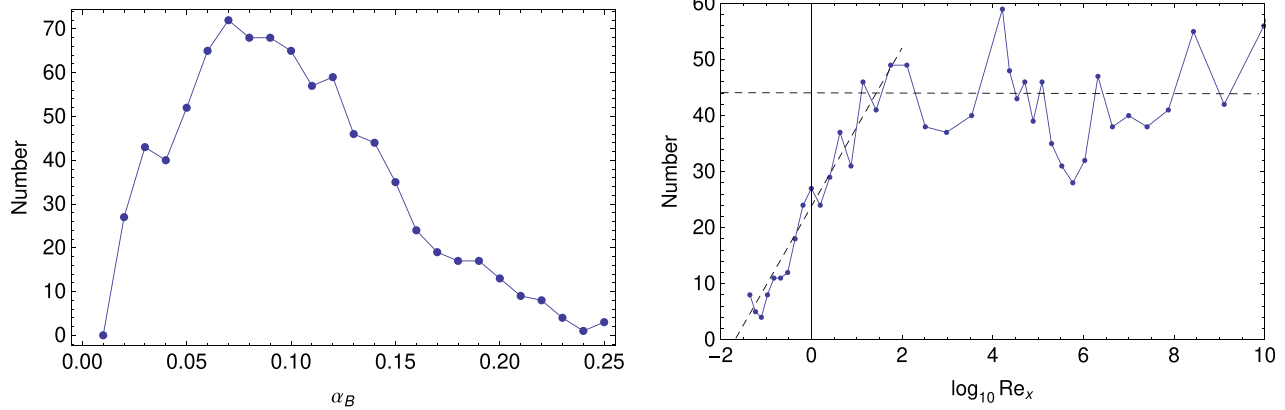


FIG. 11. Left figure: PDF of the boundary layer thickness parameter $\alpha_B = 0.16 R_x^{-1/7}$ (with $\delta(x) = \alpha_B x$) obtained from the constraint $Q(\alpha_B, \mu_B, R, \eta_P, \kappa; \eta) = \text{cst}$ by selecting values of the parameters such that the dispersion around $Q = 1$ is $\sigma_Q < 0.003$. Right figure: direct PDF of the Reynolds number R_x under the same conditions, showing a clear transition around $R_x = 1$ for $\delta_0 = 0.16$.

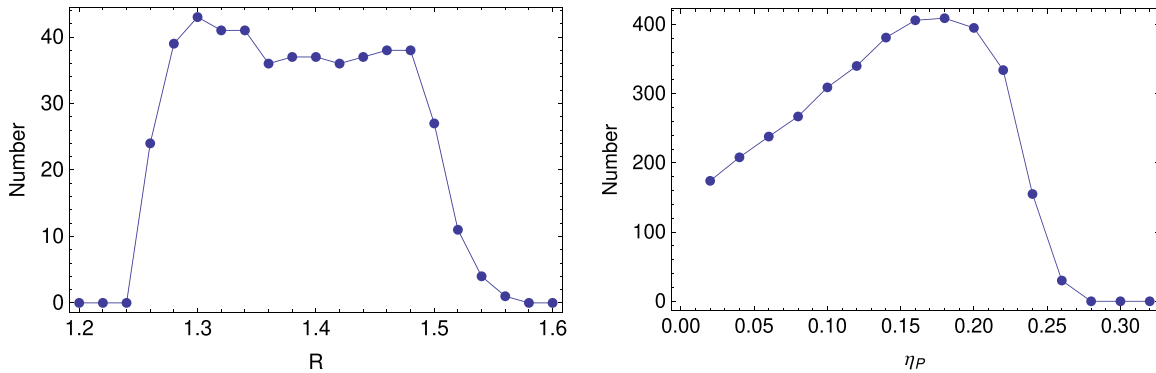


FIG. 12. Left figure: PDF of the values of the ratio $R = \sigma_u/\sigma_v$ satisfying the equation $Q(R, \eta) = 1$ with a standard deviation $\sigma_Q < 0.002$. The initial values were uniformly distributed between 1.2 and 1.6. Right figure: PDF of the values of η_P which is the position of the maximum of σ_v^2 in our theoretical solution Eq. (51). This PDF is obtained from $\sigma_Q < 0.007$ from initial values of η_P uniformly distributed between 0 and 0.4.

An example of the PDF of η_P is shown in Fig. 12 (right). It shows a well-defined peak of probability. However, contrary to what happens for the other parameters, this peak depends on the chosen limit σ_{QL} and varies from $\eta_P = 0.12$ ($\sigma_Q < 0.002$, 490 values) to $\eta_P = 0.2$ ($\sigma_Q < 0.01$, 6432 values). These values agree with the range observed for η_P in laboratory and numerical experiments on boundary layers.

4. PDF and new theoretical prediction of the Karman constant

We show in Fig. 13 an example of the $Q(\eta)$ profiles obtained by varying κ for fixed values of the other parameters. The obtained behavior suggests that a new theoretical prediction for κ is possible from the mere equation $Q = 1$, without resorting to the general argument used in Sec. V. Actually, the new result obtained here (as we shall see, a probability peak at $\kappa = 0.4$) provides us with a full justification of this argument.

In order to derive a new possible theoretical prediction for the Karman constant κ , we have performed another run with an enlarged

interval for the initial values $0.1 < \kappa < 0.5$ (with 116 480 different combinations of the parameters). For this run, the $\mu_B(R)$ function obtained for $\sigma_Q < 0.001$ reads

$$\mu_B = R_0 - 2.09 (R - R_0) + 3.83 (R - R_0)^2, \tag{56}$$

with $R_0 = 1.353$. It is in good agreement with the previous determinations of this function.

The resulting PDF of κ is given in Fig. 14. It shows a well-marked probability peak at $\kappa = 0.40$ with width ± 0.02 , which is just the range of its experimentally observed values. This is a remarkable result in support of our direct derivation of its value from the turbulent intensity ratio $\kappa = 1/R^3 \approx 0.4$. The effect of the Karman constant in the function $Q(\kappa; \eta) = 1$ comes from its intervention (as $1/\kappa^2$) in the solution of RANS equations given by Eq. (52) for σ_{uv} . It is itself a manifestation of the mean velocity contribution in the RANS equation and, therefore, of the log-law of the wall for the streamwise mean velocity U . In other words, it is the very Karman constant κ of the log-law for which we have found here a theoretical prediction, not only a secondary effect of its value.

21 June 2024 15:01:21

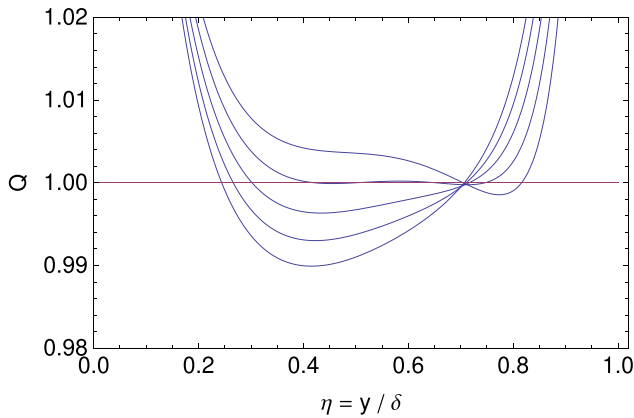


FIG. 13. Profiles of the function $Q(\eta)$ along the direction normal to the wall obtained by varying the Karman constant κ for fixed values of the other parameters. The theoretical expectation is a flat profile $Q=1$. The profiles are plotted for $\kappa = (0.37, 0.38, 0.39, 0.40, 0.41)$ from bottom to top, showing a flat profile for $\kappa = 0.40$ in the range $\eta \approx (0.4 - 0.8)$. The other parameters are in this case $\alpha_B = 0.045$, $\mu_B = R = 1.345$, $\eta_p = 0.15$.

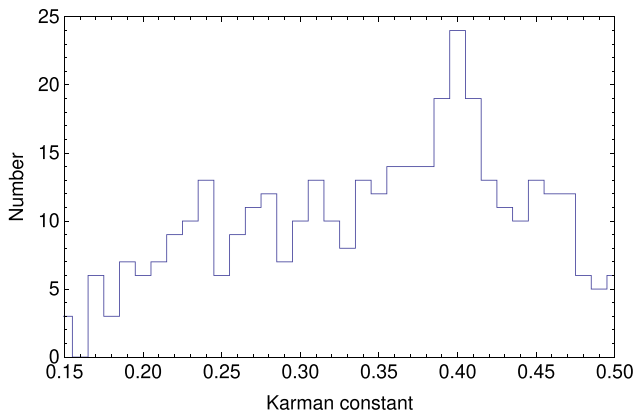


FIG. 14. PDF of the values of the Karman constant κ satisfying the equation $Q(\kappa; \eta) = 1$ with a standard deviation $\sigma_Q < 0.008$. The initial values of κ were uniformly distributed between 0.1 and 0.5.

This result supports a theoretical numerical value 0.4 ± 0.03 of the Karman constant but not yet the full and more general relation $\kappa = 1/R^3$. We have therefore constructed the PDF of the variable $g = \kappa R^3$ from the same set of initial values. The result is given in Fig. 15 for $\sigma_Q < 0.001$ and shows a well-defined probability peak around $g = 1$, i.e., $\kappa = 1/R^3$. When the chosen limit σ_{QL} increases, one finds mean values slightly smaller than 1, probably as a result of the bias introduced by keeping values of $Q \neq \text{cst}$. However, the predicted PDF is, strictly, the limit when $\sigma_Q \rightarrow 0$ of the σ_Q dependent PDFs. For $\sigma_Q < 0.0005$, we find $\kappa R^3 = 0.994 \pm 0.039$ (error on the mean) with a dispersion $\sigma_g = 0.146$.

We conclude that the macroscopic QHO v -Schrödinger equation derived in the scale-relativity theory not only predicts the typical value $\kappa = 0.4$ and its possible fluctuations ± 0.03 but also the full relation $\kappa = 1/R^3$ (that we previously derived from a general physics argument).

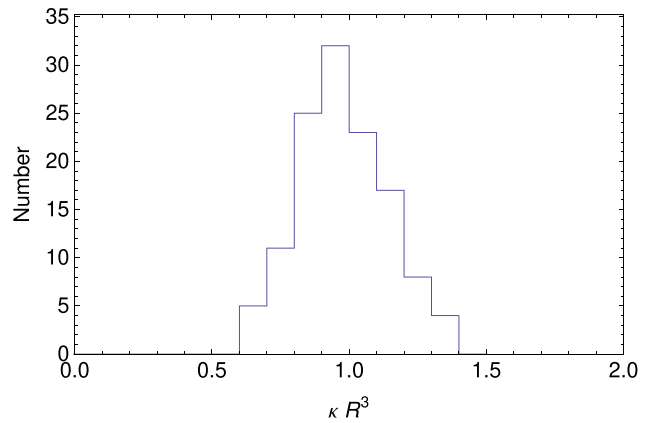


FIG. 15. PDF of the variable $g = \kappa R^3$ satisfying the equation $Q(\kappa; \eta) = 1$ with a standard deviation $\sigma_Q < 0.001$. The initial values of κ were uniformly distributed between 0.1 and 0.5 and those of R between 1.25 and 1.43. The mean value is $g = 0.982 \pm 0.014$ (error on the mean) with a standard deviation $\sigma_g = 0.157$, thus strongly supporting the relation $\kappa = 1/R^3$ to within $\approx 1\sigma$.

F. Channels and pipes

Channels and pipes deserve a special treatment since in their case the equation $Q = 1$ takes a different form. Indeed, the thickness of the turbulent region is no longer dependent on x but must now be considered constant and equal to the half-distance between the plates for channels and to the radius for cylindrical pipes. Therefore, $\eta = y/\delta$ no longer depends on x , so the second pressure equation vanishes, $k_{uv} = 0$. In this case, one finds a simplified expression

$$Q_o = 2 \delta \eta \sqrt{k_{vo}} (n_u - n_v) \sqrt{1 + \frac{1}{T^2} \frac{\sigma_{uvo}}{\mu_B^2 \sigma_{vo}^3}}, \quad (57)$$

while $2 \delta \eta \sqrt{k_{vo}} = \sqrt{1 + 4a_p^2} \sigma_{vo}$ and $\sigma_{uvo} = \rho R \mu_B^2 \sigma_{vo}^2$. Consequently, setting $\delta n = n_u - n_v$, one finds an explicit solution for μ_B given by

$$\mu_B^2 = \frac{(1 + 4a_p^2)^{1/2}}{[(Q_o/\delta n)^2 - (a_p^2 + 1/4)(1 - R^2)^2]^{1/2}} \frac{\sigma_{uvo}}{\sigma_{vo}^2}, \quad (58)$$

and for the correlation coefficient of velocities,

$$\rho = \frac{[(Q_o/\delta n)^2 - (a_p^2 + 1/4)(1 - R^2)^2]^{1/2}}{R(1 + 4a_p^2)^{1/2}}. \quad (59)$$

This expression for ρ is independent of the scaled distance $\eta = y/\delta$ to the wall, so we theoretically predict that the velocity correlation coefficient should be constant in the range relevant to our solutions for the Reynolds stresses ($0.2 < \eta < 0/7$).

Another difference for channels and pipes compared with plane boundary layers is the expression for the σ_{uv} profile. Its expression according to Lee and Moser³⁷ is $1 - y^+/Re_\tau - 1/\kappa y^+$, which in terms of large scale variables becomes

$$\sigma_{uvo} = 1 - \eta - \frac{1}{\kappa Re_\tau \eta}. \quad (60)$$

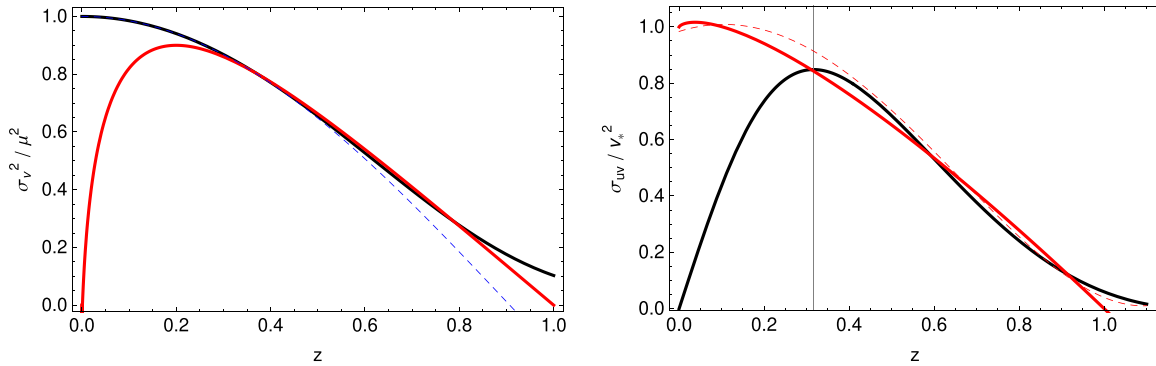


FIG. 16. Comparison between the theoretically predicted Reynolds stresses in the free turbulent jet (black curves) and in the flat plate turbulent boundary layer (red curves). The Reynolds shear stresses σ_{uv} are solutions of the continuity and RANS equations,¹⁰ for the jet and Eq. (52) for the boundary layer. The red dashed curve is a polynomial fit of (EJ) data. The Reynolds stresses σ_v^2 are solutions of the QHO v -Schrödinger equation: stretched cosine solution Eq. (61) for the jet and Eq. (51) for the boundary layer. The blue dashed curve is the cosine solution without the stretching term, which is valid in the jet central region. A double scaling is applied in order to manifest the similarity of the solutions (see the text).

However, we encounter a new problem here, since we expect $Q = \kappa_0 Q_0 = 1$ while the exact value of κ_0 , which we have found to be close to one for boundary layers, is unknown. Contrary to the boundary layer case, we cannot use here the constraint $Q = \text{cst}$. Using $\kappa_0 = 1$, we recover the same kind of results as in the BL case, but our theoretical expectation for μ_B becomes less precise in the channel and pipe cases. We intend to perform a specific study of these flows in a forthcoming work (Nottale and Lehner, in preparation).

VIII. SIMILARITY BETWEEN THE TURBULENT JET AND THE TURBULENT BOUNDARY LAYER

Another way to obtain more directly the amplitude of the Reynolds stress along the direction normal to the wall comes from the existence of a deep analogy between the turbulent jet and the boundary layer. Using this universality, we can directly use the result already obtained for the jet¹⁰ and apply it after scaling to the FPBL.

A. Universality of Reynolds stress profiles

Let us compare the theoretical solutions for the Reynolds shear stress, derived from the RANS and continuity equations, and for the radial/normal Reynolds stress, derived from the QHO v -Schrödinger equation, in the two cases of turbulent round jet and turbulent flat plate boundary layer (which can be generalized to channels and pipes).

We have obtained in Ref. 10 precise solutions for the mean velocities U and V and for the Reynolds shear stress $\sigma_{uv} = \eta U^2 - UV$ in the turbulent round jet, by matching inner solutions to the Landau exact laminar outer solution.¹⁴ The radial Reynolds stress has been theoretically derived as solution of the k_v equation:

$$\sigma_{jv}^2 = \mu^2 U_C^2 \cos\left(\frac{\sqrt{3}z}{1 + a_4 z^4}\right), \tag{61}$$

where U_C is the mean centerline velocity and $z = r/\delta = r/(\alpha x)$ is the normalized radial distance and where the amplitude $\mu = (0.20 \pm 0.015)$ and the coefficient $a_4 = 0.18$ have also been theoretically derived from the QHO v -Schrödinger equation.

In the present paper, we have obtained solutions for the same quantities in the turbulent boundary layer. These solutions are

expressed in terms of the wall-friction velocity $v_* = \sqrt{\sigma/\rho}$ as $\sigma_v^2 = \mu_B^2 v_*^2 \sigma_{v0}^2$ and $\sigma_{uv} = v_*^2 \sigma_{uvo}$. The boundary conditions are very different between the jet and the boundary layer as regards mean velocities, whose variations are reversed, and as regards the central region, since the flow behavior in the BL when $y \rightarrow 0$ becomes strongly dependent on the viscosity. However, both systems come under the boundary layer approximation of the RANS equations and, in the scale-relativity approach to turbulence developed here, are described by the same v -Schrödinger equation.

We therefore expect the two flows to be similar in regard to the turbulent fluctuations in the median and edge regions once proper scaling is applied.

First, the distance to be used is naturally the distance ratio to the edge $z = \eta = y/\delta = y/(\alpha_B x)$ for the BL and its equivalent in the jet, $z = r/\delta = r/(\alpha x)$. The analogy is made with the turbulent round jet since its scaling in function of the radial distance is $\sim x$ as the turbulent BL while the plane jet would be $\sim \sqrt{x}$, like the laminar BL.

Second, we expect from our analysis that a velocity v_{j*} could be defined for the turbulent jet in analogy with the BL velocity v_* . Such a characteristic velocity should be such that $\sigma_v^2 = \mu_0^2 v_{j*}^2 \sigma_{v0}^2$ and $\sigma_{uv} = v_{j*}^2 \sigma_{uvo}$ for the jet.

We show in Fig. 16 a comparison of the theoretically predicted profiles after such a double scaling, for $v_{j*} = 0.145 U_C$. An excellent agreement is indeed obtained between the σ_v^2 profiles in the range $z \approx (0.2 - 0.9)$, i.e., in about the outer 3/4th of the turbulent region. Since $p = -\sigma_v^2$ in both cases, this means that the potential in the v -Schrödinger equation is the same in this range. This result definitively proves the identity of the turbulent fluctuation equations in the median region of the turbulent domain. Laboratory and numerical experiments fairly support this result, as can be seen in the examples of Fig. 17.

B. Consequence: Prediction of BL turbulent intensity amplitude from jet amplitude

This remarkable similarity between the jet and the boundary layer turbulent fluctuations allows one to directly derive the amplitude of

21 June 2024 15:01:21

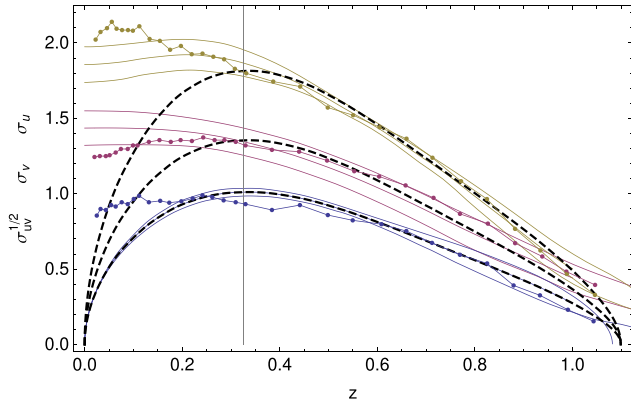


FIG. 17. Comparison between the Reynolds stresses in the free turbulent jet and in the flat plate turbulent boundary layer. The blue, magenta, and brown continuous lines are measurements of, respectively, $\sigma_{uw}^{1/2}$, σ_v , and σ_u in the free jet by Panchapakesan and Lumley (PL),³⁹ Hussein *et al.* [Hussein, Capp, George (HCG)],⁴⁰ and their mean. They have been normalized by a velocity $v_{j*} = 0.14 U_C$, where $U_C = U_0 a_0/x$ is the mean centerline velocity and plotted in function of the scaled variable $z = r/\alpha x$. The irregular blue, magenta, and brown lines with points are measurements of the same quantities in a flat plate boundary layer by Shafi and Antonia,²⁶ plotted in function of $z = y/\delta$. The black dashed curves show $v_0(z)/v_{j*}$, $R v_0(z)/v_{j*}$, and $R^2 v_0(z)/v_{j*}$ from $v_0(z) = \sigma_{uw}^{1/2}$ given by the mean of PL and HCG measurements, with $R = \sigma_u/\sigma_v = 1.35$.

the BL turbulent intensity μ_B along the direction normal to the plate from the jet radial amplitude μ_j . It reads

$$\mu_B = \mu_j \frac{\sigma_{v_0}^J}{\sigma_{v_0}^B} \sqrt{\frac{\sigma_{uw}^B}{\sigma_{uw}^J}}, \tag{62}$$

where the index J stands for the jet and B for the boundary layer.

Using our solutions for the jet¹⁰ and for the boundary layer (present paper), we find a theoretical prediction for the ratio μ_B/μ_j , which is shown in Fig. 18 for various values of the parameters. As expected, it

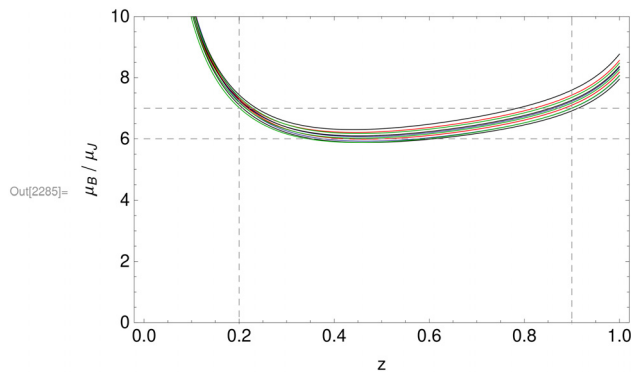


FIG. 18. Theoretical expectation of the ratio μ_B/μ_j between the boundary layer and the round jet turbulent intensity amplitudes, as given by Eq. (62). The variable z denotes the normalized distance along the radial direction $z = r/(\alpha x)$ for the round jet and along the direction normal to the wall $z = y/(\alpha_B x)$ for the boundary layer, where x is the axial direction along the streamwise velocity. The different curves correspond to different values of the parameters: $\kappa = (0.37, 0.4, 0.43)$ (blue curves); $\eta_p = (0.15, 0.175, 0.20)$ (red curves); $\alpha_B = (0.025, 0.045, 0.065)$ (black curves); $\alpha = (0.195, 0.205, 0.215)$ (green curves).

is almost constant in function of the variable $z = r/\alpha x$ (round jet) and $z = y/\alpha_B x$ (BL) in the relevant range $z = (0.3 - 0.8)$. Its value, $\mu_B/\mu_j \approx 6 - 7$, yields a theoretical explanation for the observed ratio $(0.14 - 0.15)$ between v_{j*} and U_C (see Fig. 17).

From the theoretically predicted range $\mu_j = 0.20 \pm 0.015$,¹⁰ one obtains $\mu_B = 1.35 \pm 0.15$, in good agreement with its direct determination.

IX. THEORETICAL PREDICTION OF THE VELOCITY CORRELATION COEFFICIENT

One of the main mysteries of turbulence is the universality of the correlation coefficient of velocities, which is known to be $\rho \approx 0.4$ for all shear flows.^{4,5} We have given a theoretical explanation for this value in the turbulent round jet case, where we have found $\rho = 1/R^3$.¹⁰ We are now in position to generalize this result to many other flows, such as plane boundary layers, channels, and pipes.

The first and shortest way to obtain the result $\rho = 1/R^3 \approx 0.4$ consists of using the similarity found above between the turbulent round jet and the plane boundary layer, which implies that the jet result is also valid for boundary layers. The new information brought here is the identity between the Karman constant and the velocity correlation coefficient, both being given by R^{-3} to lowest order, in agreement with their common experimentally measured numerical value ≈ 0.4 .

There is another direct way toward this result: the general form given to the Reynolds stresses using the characteristic velocity v_* , which we have shown to be valid for both the turbulent jet and boundary layers (see Fig. 17), allows us to now solve the problem in a fast way.

Indeed, the coefficient of correlation of velocities is given by

$$\rho = \frac{\sigma_{uv}}{\sigma_u \sigma_v} = \frac{\sigma_{uv}}{R \sigma_v^2} = \frac{1}{R \mu_B^2} \frac{\sigma_{uvw}}{\sigma_{v_0}^2}. \tag{63}$$

With the normalized Reynolds stresses $\sigma_{uvw} \sim 1$ and $\sigma_{v_0}^2 \sim 1$ around $z \approx 0.2$ (by construction), we get $\rho \approx 1/(R \mu_B^2)$, i.e., to lowest order, knowing that $R \approx \mu_B \approx R_0 = 1.35$,

$$\rho \approx \frac{1}{R_0^3} \approx 0.4, \tag{64}$$

which is the well-known universal experimental value of the correlation coefficient for all shear flows.⁴ This value is therefore now theoretically established for round jets, plane boundary layers, channels, and pipes (Ref. 10 and present paper).

In a more elaborate way, using our explicit expressions for the Reynolds stresses, the coefficient of correlation of velocities reads as follows for the flat plate turbulent boundary layer:

$$\rho = \frac{\sigma_{uv}}{R \sigma_v^2} = \frac{\sqrt{\eta_p} \sin(a_p \ln \eta_p) \left(1 - \eta - \frac{\alpha_B}{\kappa^2} \eta \ln \eta\right)}{R \mu_B^2 \sqrt{\eta} \sin(a_p \ln \eta)}. \tag{65}$$

Using the analytical expression we have found for μ_B , we obtain quasi-constant profiles $\rho \approx 0.4$ for the coefficient of correlation in the relevant interval $\eta \approx (0.2 - 1)$, as shown in Fig. 19, with variations $< \approx \pm 0.03$ depending on the values of the parameters.

In another way to get this result, the equation $Q = \text{cst}$ can also be directly reformulated in terms of the correlation coefficient ρ .

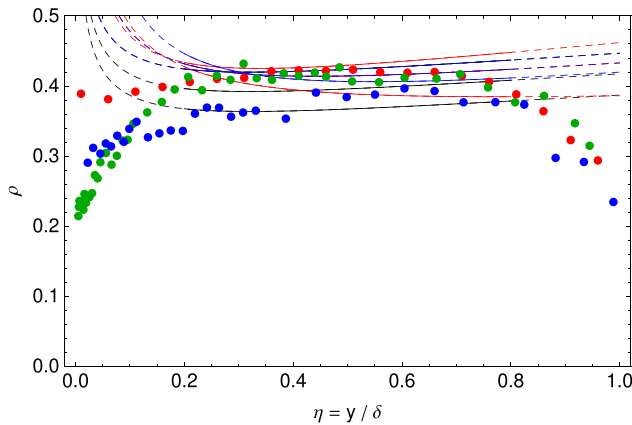


FIG. 19. Predicted profile of the correlation coefficient of the (u, v) velocities, for various values of the parameters. We find that it is practically constant on the relevant range $\eta \approx (0.2 - 0.8)$ where the approximation $R = \text{cst}$ holds. The values of the parameters are $\kappa = 0.4$, $R = (1.34, 1.37, 1.4)$, black curves; $\alpha_B = (0.01, 0.045, 0.07)$, red curves; $\eta_p = (0.12, 0.16, 0.20)$, blue curves. The variation with κ is very weak, as expected from the direct reformulation of the equation $1/Q = \text{cst}$ [Eq. (68)], which no longer depends on it. We compare this almost constant theoretical profile to values derived from experimental data: Sillero *et al.*,⁴¹ red points; Shafi and Antonia,²⁶ blue points; Gungor *et al.*,⁴² green points.

The resulting equation no longer depends on σ_{uv} , and therefore on the Karman constant κ . The decorrelation angle θ is given by $T = \tan(2\theta)$, which takes now a new form in terms of R and ρ :

$$T = \frac{2R}{R^2 - 1} \rho, \tag{66}$$

and also

$$\begin{aligned} k_{u0} &= k_{v0} - k_{uvo} \frac{1}{T} \left(1 + \frac{1 - T^2}{\sqrt{1 + T^2}} \right), \\ k_{v0} &= k_{v0} - k_{uvo} \frac{1}{T} \left(1 - \frac{1 - T^2}{\sqrt{1 + T^2}} \right). \end{aligned} \tag{67}$$

We set, as before, $W_{u0} = 1/\sqrt{k_{u0}}$ and $W_{v0} = 1/\sqrt{k_{v0}}$. Then, we obtain a new expression for the equation $S = 1/Q = 1$:

$$S_0 = \frac{\sigma_{v0}}{\alpha_B \kappa \eta (R^2 - 1) \sqrt{1 + T^2}} ((n_u + 1/2)W_{u0} - (n_v + 1/2)W_{v0}), \tag{68}$$

with $S_0 = 2\kappa_0 S$.

We find that $S = \text{cst}$ for a limited range of values of the parameter $T \approx (1.18 - 1.20)$, as can be seen in Fig. 20. From this range, we find $\rho = (0.36 - 0.41)$ for $R = (1.35 - 1.40)$, which is compatible with the interval of values obtained from directly inserting the function $\mu_B(r, a, p, k)$ in the ρ expression Eq. (65).

X. DISCUSSION

Although many new results have been obtained from the scale-relativity theory of turbulence, such as theoretical predictions of the Karman constant value and of its variations, of the normal Reynolds stress profile and of its amplitude, and of the velocity correlation

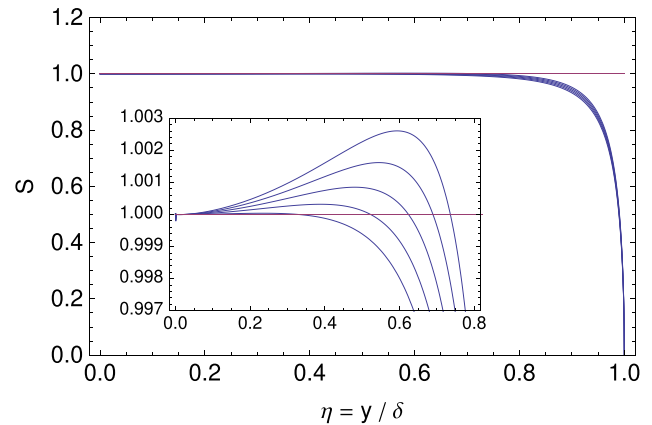


FIG. 20. Profile $S(\eta)$ from Eq. (68) obtained for $T = (1.18, 1.185, 1.19, 1.195, 1.20)$, where $T = 2R\rho/(R^2 - 1)$ and $n_u = 2, n_v = 1, \eta_p = 0.20$, and $\alpha_B = 0.045$. It remains almost constant as theoretically expected, here on the range $\eta = (0, 0.8)$. The inset is an enlarged view showing that the small differences with $S = 1/Q = 1$ are of order a few 10^{-3} .

coefficient, there still remain a few problems and open questions that require further work.

A first problem is that, as in the turbulent jet case, the k_u equation cannot be used in the boundary layer study since it yields a repulsive harmonic oscillator solution for the u velocity fluctuations on most of the normal profile. We have circumvented this problem by setting $\sigma_u = R\sigma_v$ following the argument of Tennekes and Lumley⁴ and using only the k_v and k_{uv} equations. However, this problem seems to point to the fact that the axial component of the velocity-space Schrödinger equation, i.e., along the streamwise flow, is incorrect or incomplete. A more thorough analysis of this problem will be needed.

Another possible drawback concerns the k_v equation, which depends on a parameter B_0 , which we have assumed to be constant. Under this hypothesis, this parameter is replaced by the equivalent parameter a_p , which can be finally expressed in terms of η_p , the position of the maximum of $\sigma_v(\eta)$. This constancy hypothesis is strongly supported by the excellent agreement obtained between our theoretical profile solution of the k_v equation and the experimental and numerical data. However, both the consistency of the values of B_0 corresponding to its various constituents and its constancy may be questioned and should be studied in more detail.

Using Landau's remark that there is no fixed available scale in the boundary layer problem, so only y can be used, has led us to suggest that the natural length scale in the axial direction is $L_x = y$, so $L_y = R^{-3}L_x$ from the unity of the macroscopic Planck constant, implying a Karman constant $\kappa = R^{-3} \approx 0.4$. One could argue against this reasoning that L_x should be defined up to another unknown numerical constant, i.e., $L_x = ky$. However, we have also obtained the same result from the PDF of the variable $g = \kappa R^3$, which shows a well-defined probability peak at $g = 1$. Since this PDF is derived from the constraint $Q = \text{cst}$, i.e., directly from the v -Schrödinger equation (which is itself a reformulation of the Navier–Stokes equations in the turbulent K41 regime), we consider that this result is in support of our general physics argument à la Landau.

Further studies are needed to tackle a few questions that have not been addressed in the present work, such as that of the lateral

Reynolds stress profile $\sigma_w^2(\eta)$ or that of the origin of the possible values of Coles's wake law parameter, which is known only empirically.

Another incompleteness concerns the values of the QHO quantum numbers in the $Q = 1$ equation, which we have taken to be $n_u = 2$ and $n_v = 1$ as representing the most probable excited state. A full solution would involve performing the same analysis for all states and combining them according to their probability densities predicted by statistical physics.

An interesting open question is that of the universality of Reynolds stress profiles. We have found such a universality concerning turbulent jets, boundary layers, channels, and pipes (and possibly other sheared flows), which is understood as coming from the universality of QHOs, even though the parameters in our k_v equation may differ from one flow to the other. Another form of universality has been suggested for dissipation-scaled wall turbulence by Tang and Antonia,⁴³ which is difficult to compare to ours, since it applies to different scales.

We intend to tackle these open questions in a forthcoming study. We shall also analyze in more detail the theoretically predicted dependence of various quantities like κ and ρ in function of other parameters such as α_B (and therefore the Reynolds number). This dependence, which we have found to be small, may offer an explanation for the experimentally observed behavior of these quantities, which show both a global universality (e.g., $\kappa \approx 0.4$) and small variations possibly depending on flow conditions (e.g., $\kappa = 0.37, 0.39$, and 0.41 , respectively, for channels, boundary layers, and pipes⁶). Our theoretical predictions offer the ability to test for these variations by searching for correlations with the relevant parameters in experimental and numerical data.

XI. CONCLUSION

We have applied in the present work the scale-relativity approach to the plane turbulent boundary layer problem, which concerns also, to some extent, channels and pipes. In our analysis, we have concentrated on the outer region far from the wall $\eta = y/\delta \gg \approx 0.1$, which allows us to neglect the effect of viscosity. Moreover, the intermediate region $0.1 < \eta < 0.3$ has the advantage that it can be still well described by the "law of the wall" as regards the mean velocity in boundary layers (and even farther for channels and pipes). This allows matching of inner and outer solutions.

In the scale-relativity theory, we have shown that the effect of a non-differentiable and fractal space or medium is to transform the fundamental equation of dynamics into a macroscopic Schrödinger-like equation. Applied to fluid mechanics and in velocity-space,¹¹ this means that the Navier–Stokes equations, once derived in time and re-integrated in velocity, are transformed in terms of a v -Schrödinger equation in which the potential is a manifestation of the pressure gradient. We have shown that it takes in an universal way the form of a harmonic oscillator potential.^{10,16}

Under the boundary layer approximation, which is valid in many flows, such as jets, flat plate boundary layers, channels, and pipes, the pressure is the opposite of the Reynolds stress, i.e., $p = -\sigma_v^2$. The potential in the v -Schrödinger equation is, therefore, given by the derivatives of the normal Reynolds stress, which ensures solving the closure problem in these cases.

In this framework, we have been able to theoretically predict quantities that are fundamental to turbulence, such as the Karman constant κ , the ratio of turbulent intensities $R = \sigma_u/\sigma_v$, the profile and amplitude μ_B^2 of the Reynolds stress σ_v^2 along the direction normal

to the wall, and the coefficient of correlation of velocities ρ . These predictions, according to which $\mu_B = R \approx 1.35$ and $\kappa = \rho = R^{-3} = 0.4$ to lowest order, are in fair agreement with the data from observations and from laboratory and numerical experiments. In particular, the well-known puzzle of the universality of the value $\rho \approx 0.4$ of the velocity correlation coefficient in all shear flows⁴ has now received a beginning of explanation, being theoretically predicted by the scale-relativity/macroscopic Schrödinger equation approach for round jets,¹⁰ plane boundary layers, channels, and pipes.

AUTHOR DECLARATIONS

Conflict of Interest

The authors have no conflicts to disclose.

Author Contributions

Laurent Nottale: Conceptualization (lead); Validation (lead). **Thierry Lehner:** Conceptualization (equal).

DATA AVAILABILITY

The data that support the findings of this study are available from the corresponding author upon reasonable request.

APPENDIX A: PROPERTIES OF THE REYNOLDS STRESS SOLUTION

We have found a solution to the v -Schrödinger equation for the Reynolds stress σ_v^2 , which reads

$$\sigma_v^2 = A \mu_B^2 v_*^2 \sqrt{\eta} \sin(a_P \ln \eta). \tag{A1}$$

The normalized coordinate is $\eta = y/\delta$, where y is the distance normal to the wall and δ the width of the turbulent zone. Calling η_P the position of the peak of this function, the normalization factor is given by $A^{-1} = \sqrt{\eta_P} \sin(a_P \ln \eta_P)$, so the peak value is $\sigma_{vP}^2 = \mu_B^2 v_*^2$,

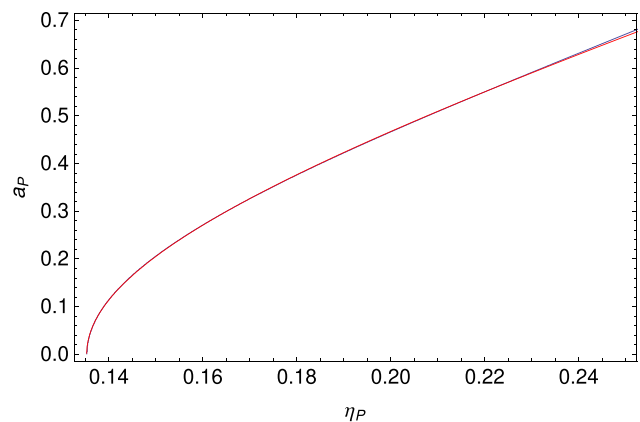


FIG. 21. Variation of the parameter a_P in the reduced expression of the Reynolds stress $\sigma_{vP}^2 = \sqrt{\eta} \sin(a_P \ln \eta)$ in function of the position η_P of its maximum. The blue curve results from a numerical calculation while the red curve is the analytical approximation Eq. (A2).

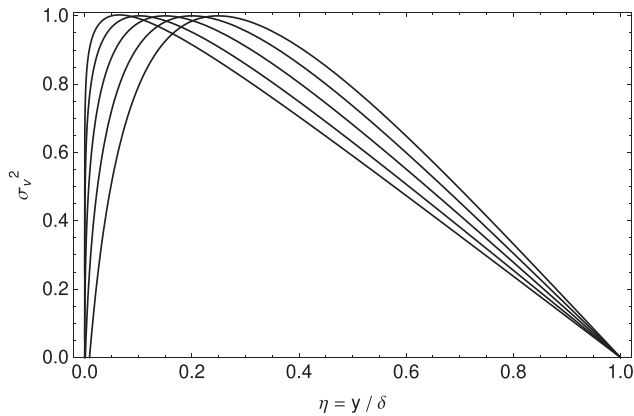


FIG. 22. Solutions of the QHO v -Schrödinger equation for the Reynolds stress profiles σ_v^2 [Eq. (A1)]. The function is normalized to $\sigma_v(\eta_p) = 1$, where η_p is the position of its maximum, and it is plotted for various values of this position, $\eta_p = 0.05, 0.10, 0.15, 0.20$, and 0.25 .

which defines the amplitude μ_B . The parameter a_p is given in function of η_p to an excellent approximation by

$$a_p = 3.172 \sqrt{\eta_p^2 - \eta_{p0}^2}, \tag{A2}$$

where $\eta_{p0} = 0.13529$ (see Fig. 21). For $\eta_p < 0.135$, the normalized expression remains valid with an imaginary parameter $a_p = ia$. In this case, the reduced Reynolds stress may also be written in terms of real numbers as $\sigma_{v0}^2 = \sqrt{\eta/\eta_p} \times \sinh(a \ln \eta) / \sinh(a \ln \eta_p)$. Our solution for the Reynolds stress is plotted in Fig. 22 for various values of the peak position η_p .

APPENDIX B: VARIOUS SOLUTIONS OF THE EQUATION $Q = cst$

We numerically solve the equation $Q(R, \mu_B, \eta_p, \alpha_B, \kappa; \eta) = 1$ by keeping only the values of the parameters for which the standard deviation σ_Q with respect to the flat profile $Q(\eta) = 1$ are small (typically $\sigma_Q < 0.002$) in the relevant range $\eta = 0.3 - 0.7$.

The expression for Q [Eq. (50)] involves the Reynolds shear stress, σ_{uv} , for which various theoretical solutions have been proposed.²² The simplest is $\sigma_{uv} = 1 - \eta$.⁴ We have obtained a more elaborate solution, which reads

$$\sigma_{uv} = v_x^2 \left(1 - \eta \left(1 - \frac{\alpha_B}{\kappa^2} \ln \eta \right) \right), \tag{B1}$$

while some experimental data yield slightly higher values (see Fig. 1 and references in its caption). We have considered these various possibilities in searching for a relation between the shear stress amplitude μ_B along the direction normal to the wall and the turbulent intensity ratio $R = \sigma_u / \sigma_v$.

We consider here the results of a run made with $\kappa = 0.4$ and the other parameters in the ranges $R = (1.2 - 1.6)$, $\mu_B = (0.8 - 1.6)$, $\alpha_B = (0.03 - 0.06)$, and $\eta_p = (0 - 0.4)$.

When using the approximate expression for $\sigma_{uv} = 1 - \eta$, a fit of the parameter subset such that $\sigma_\xi < 0.002$ yields the following,

with a high statistical significance (Student's $t > 45$ for the R coefficients):

$$\mu_B = 14.084 - 16.94R + 5.57R^2 - 5.34\alpha_B + 37.11\alpha_B^2 + 0.423\eta_p. \tag{B2}$$

Neglecting the dependence of μ_B on α_B and η_p , which remains small, we obtain

$$\mu_B(R) = R_0 - 2.18(R - R_0) + 5.5(R - R_0)^2, \tag{B3}$$

where $R_0 = 1.33$ in that case.

When using the polynomial fit of [Erm and Joubert (E)] data for σ_{uv} (see Fig. 1), a fit of the parameter subset such that $\sigma_\xi < 0.002$ yields the following, with a high statistical significance (Student's $t > 70$ for the R coefficients):

$$\mu_B = 12.182 - 13.00R + 3.93R^2 - 3.44\alpha_B + 23.0\alpha_B^2 - 2.79\eta_p + 7.82\eta_p^2. \tag{B4}$$

Neglecting the small dependence of μ_B on α_B and η_p , we obtain

$$\mu_B(R) = R_0 - 2.15(R - R_0) + 4.0(R - R_0)^2, \tag{B5}$$

where $R_0 = 1.38$ in that case.

APPENDIX C: ANALYTIC SOLUTION FROM POWER SERIES

1. Power series of function Q

Another way to obtain solutions for the equation $Q = 1$ consists of expanding Q in power series. Since we expect Q to be a constant independent from η , a linear expansion $Q = A(R, \mu_B) + B(R, \mu_B)(\eta - \eta_0)$ is sufficient and the searched solution is given by the slope cancellation $B(R, \mu_B) = 0$. Solving for this equation yields the solution $\mu_B = \mu_B(R)$, which depends also slightly on (α_B, η_p , and κ).

Since we already know that R lies in a restricted range $R \approx (1.3 - 1.4)$, we use linear expansions for R and for μ_B . The power series is performed in terms of $(R - R_0)$, $(\mu_B - \mu_{B0})$, and $(\eta - \eta_0)$ for various numerical values of the three remaining parameters, α_B, η_p , and κ . After expansion, it takes the form

$$Q = (a_0 + b_0R + c_0\mu_B + d_0R\mu_B) + (a + bR + c\mu_B + dR\mu_B)\eta. \tag{C1}$$

Thus, the equation $Q = 1$ is translated into the slope cancellation equation $(a + bR + c\mu_B + dR\mu_B) = 0$, which leads to the searched solution:

$$\mu_B(R) = -\frac{a + bR}{c + dR}. \tag{C2}$$

We have taken $\eta_0 = 0.5$, $R_0 = 1.34$, and $\mu_{B0} = 1.34$, knowing that the final result is almost independent of this choice. These operations have been performed for numerical values of α_B, η_p , and κ taken in their expected range (see caption of Fig. 23). The parameters (a, b, c, d) are found to weakly depend on these values. The result, plotted in Fig. 23, fully agrees with the previous fit method.

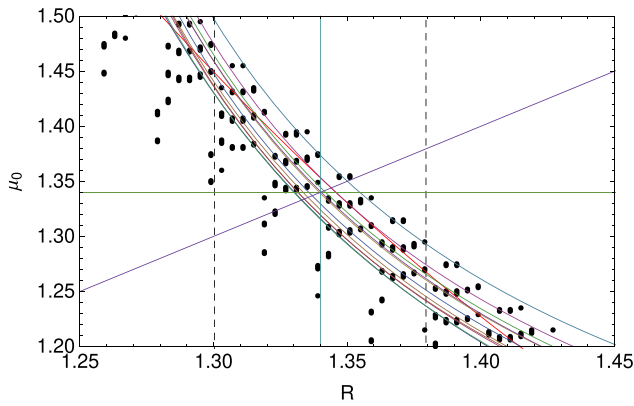


FIG. 23. Comparison between the solutions of the equation $Q = \text{cst}$ obtained by fit with those obtained by power series. The solution by fit is given by the black points, which are values of R and μ_B such that the standard deviation of Q values around $Q = 1$ is $\sigma_Q < 0.002$. The dispersion between the points mainly comes from variation between the values of α_B and η_P . They have been slightly displaced in function of the values of these parameters in order to distinguish them (see Fig. 9 for a correction of their effect). The solutions by power series are found from the cancellation of the η coefficient in the linear expansion of $Q(\eta)$. The different curves correspond to $\alpha_B = (0.03, 0.045, 0.06)$, $\eta_P = (0.15, 0.175, 0.20)$, and $\kappa = (0.37, 0.40, 0.43)$.

One finds a median solution given to lowest order by

$$\mu_B = R_0 - 2.25 (R - R_0), \tag{C3}$$

where $R_0 = 1.334$. Both the slope and the point R_0 for which $R = \mu_B$ essentially agree with the result from the fit method.

The main variation comes from R while the other variables contribute only by $\approx \pm 0.02$. In order to be more specific on this point, we have performed a power series expansion for all parameters. We verify that the quadratic terms are small with respect to the linear ones. We set $n = \eta - \eta_0$, $r = R - R_0$, $m = \mu_B - \mu_{B0}$, $a = \alpha_B - \alpha_{B0}$, $p = \eta_P - \eta_{P0}$, and $k = \kappa - \kappa_0$. For example, performing an expansion of Q around $R_0 = \mu_{B0} = 1.344$, $\eta_0 = 0.5$, $\alpha_{B0} = 0.045$, $\eta_{P0} = 0.16$, and $\kappa_0 = 0.4$ we find

$$Q = 1 - 0.026 n + 0.029 n^2 + 2.1 r - 0.59 m + 1.27 a + 3.6 p - 0.32 k, \tag{C4}$$

manifesting a very flat variation with η as expected and a small dependence on the other parameters.

2. Full order two power series

In order to get a more complete understanding of the behavior of the function $Q = Q(R, \mu_B, \alpha_B, \eta_P, \kappa; \eta)$ and of the way by which it can become constant, we have performed a full power series expansion of Q , linear in terms of η and up to order two in function of all the parameters. A full analytic form of the searched function $\mu_B = \mu_B(R, \alpha_B, \eta_P, \kappa)$ will then result from the cancellation of the η coefficient.

We have performed a power series expansion around the values $(R_0, \mu_{B0}, \alpha_{B0}, \eta_{P0}, \kappa_0) = (1.35, 1.35, 0.045, 0.16, 0.40)$, which are central with respect to the previously established possible range for these parameters. This allows us to now get an explicit form for the

dependence of the relation $m(r)$ on the other parameters. After normalization to one of the constant coefficients, we find

$$Q = 1 - 0.5037 m + 2.167 r + 1.411 a + 4.378 p - 0.277 k + 1.127 m^2 + 3.59 r^2 - 12.92 a^2 - 0.60 p^2 + 1.21 k^2 + 2.513 mr + 2.27 ma - 2.97 mp + 1.03 mk + 9.65 ra + 7.78 rp + 1.38 rk + 13.7 ap - 3.91 ak - 1.64 pk + (0.0543 + 1.618 m + 3.764 r - 1.771 a + 1.070 p + 0.632 k - 0.0376 m^2 + 10.04 r^2 - 70.93 a^2 - 8.30 p^2 - 1.52 k^2 + 7.801 mr + 24.30 ma - 1.63 mp + 1.58 mk + 48.03 ra - 0.096 rp + 5.59 rk + 43.52 ap + 27.24 ak - 2.42 pk) n. \tag{C5}$$

We express the constancy of Q by the cancellation of the coefficient of the n term. This equation is solved in terms of the function $m = m(r, a, p, k)$. We finally find a complete analytical expression for $m = \mu_B - 1.35$:

$$m = (-0.0336 + 1.596a - 0.694p - 0.357k - 13.04ak + 1.29k^2 - 14.90ap + 1.83kp) + (-2.161 - 5.079a + 1.297p + 0.421k + 62.82ak - 6.75k^2 + 48.91ap - 9.85kp) r + (4.317 - 39.45a - 2.18p - 6.36k - 177.3ak + 39.7k^2 - 249.5ap + 44.8kp) r^2. \tag{C6}$$

The resulting function and its dispersion agree with its numerical determination as given in Fig. 23. In particular, its expression for $R = \mu_B = 1.35$, $\alpha_B = 0.045$, $\eta_P = 0.14$, and $\kappa = 0.4$ in the relevant range $R = (1.3 - 1.4)$ is very close to the fit of the numerical integration given by the red curve in Fig. 8. We show in Fig. 9 the function $m(r)$ for various values of the parameters. This analytical result supports our general conclusion according to which $\mu_B \approx R$. The value for which $\mu_B = R$ is found to be more precisely $R_0 = 1.34 \pm 0.01$.

Finally, we have numerically checked the validity of this result by comparing the PDF of the standard deviation σ_Q of Q values relative to $Q = 1$ under the constraint given by Eq. (55), to the PDF obtained for all values without constraint. The result of this comparison is given in Fig. 24 and is very satisfactory. The PDF obtained while using the analytic expression for μ_B shows a well-defined peak at $\sigma_Q = 0.002$, then decreases with $\sigma_Q < 0.013$. This is in good agreement with the constraint $\sigma_Q < 0.002 - 0.005$ we have used to numerically establish the $\mu_B(R, \alpha_B, \eta_P, \kappa)$ relation.

Remark that this solution, obtained from the cancellation of the linear term of $Q(n)$, though satisfactory since agreeing with the numerical results, cannot be considered as yet optimal. Indeed, the profile with smallest dispersion around $Q = 1$ may have a slope that is small but nevertheless nonzero at $n = 0$. Actually, as can be seen in Fig. 7, the profiles for which the standard deviation σ_Q with respect to $Q = \text{cst}$ are the smallest have a W-like shape characteristic of polynomials of order at least η^4 , with a negative parabolic contribution $-\eta^2$. We have compared these profiles with their power series expression and found that a complete agreement can be obtained in every case only at order η^6 or η^8 . A more detailed analysis of this behavior will be presented in a future work. In particular, we expect to recover in an analytic way the various

21 June 2024 15:01:21

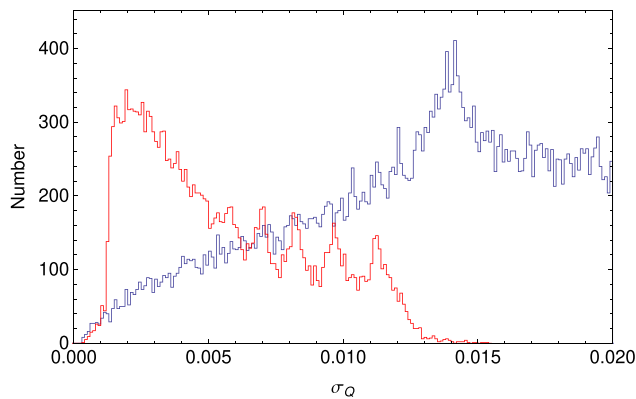


FIG. 24. Comparison between the PDFs of standard deviations σ_Q under the constraint given by Eq. (55) (red histogram) to their PDF without constraint (blue histogram). The analytic μ_B expression has been obtained by canceling the linear term $B=0$ in the power series expansion $Q = A + Bn + \mathcal{O}[n^2]$. We have cut the no constraint PDF at $\sigma_Q = 0.02$, but it actually continues without decreasing up to large values ~ 1 .

properties that have been obtained by numerical methods (PDFs of parameters and relations between them).

REFERENCES

- ¹T. von Karman, "Mechanische Ähnlichkeit und turbulenz," in *Proceedings of the Third International Congress of Applied Mechanics* (Weidmannsche Buchh., 1930), pp. 85–105.
- ²L. Prandtl, "Zur Turbulenten Strömung in Rohren und längs Platten," in *Ergebnisse der Aerodynamischen Versuchsanstalt zu Göttingen, IV Lieferung* (Oldenbourg, 1932), Vol. 4.
- ³A. N. Kolmogorov, "The local structure of turbulence in incompressible viscous fluid for very large Reynolds numbers," *C. R. Acad. Sci. URSS* **30**, 301 (1941).
- ⁴H. Tennekes and J. L. Lumley, *A First Course in Turbulence* (MIT Press, Cambridge, MA, 1972).
- ⁵S. B. Pope, *Turbulent Flows* (Cambridge University Press, 2000).
- ⁶H. M. Nagib and K. A. Chauhan, "Variations of von Kármán coefficient in canonical flows," *Phys. Fluids* **20**, 101518 (2008).
- ⁷S. Bailey, M. Vallikivi, M. Hultmark, and A. Smits, "Estimating the value of von Kármán's constant in turbulent pipe flow," *J. Fluid Mech.* **749**, 79–98 (2014).
- ⁸W. K. George, "Is there a universal log law for turbulent wall-bounded flows?," *Philos. Trans. R. Soc. A* **365**(1852), 789–806 (2007).
- ⁹G. Smart, "A base for the log law and von Karman's constant problem," *J. Hydraul. Res.* **60**(6), 935–943 (2022).
- ¹⁰L. Nottale and T. Lehner, "The turbulent jet in the scale-relativity framework," *Phys. Fluids* **36**, 045118 (2024).
- ¹¹L. de Montera, "A theory of turbulence based on scale relativity," [arXiv:1303.3266](https://arxiv.org/abs/1303.3266) (2013).
- ¹²L. Nottale, "Relativity of scales, fractal space-time and quantum potentials," in *Space-Time Geometry and Quantum Events*, edited by I. Licata (Nova Science, 2014), Chap. 5.
- ¹³L. Nottale and T. Lehner, "Turbulence and scale relativity," *Phys. Fluids* **31**, 105109 (2019).
- ¹⁴L. Landau and E. Lifchitz, *Fluid Mechanics* (Pergamon Press, Oxford, 1980).
- ¹⁵U. Frisch, *Turbulence: The Legacy of A.N. Kolmogorov* (Cambridge University Press, 1995).
- ¹⁶L. de Montera, T. Lehner, W. Mouhali, and L. Nottale, "Describing geophysical turbulence with a Schrödinger–Coriolis equation in velocity-space," *Phys. Fluids* **36**, 015136 (2024).
- ¹⁷L. Nottale, *Fractal Space-Time and Microphysics: Towards a Theory of Scale Relativity* (World Scientific, Singapore, 1993).
- ¹⁸L. Nottale, *Scale Relativity and Fractal Space-Time: A New Approach to Unifying Relativity and Quantum Mechanics* (Imperial College Press, London, 2011).
- ¹⁹L. Nottale, "Generalized quantum potentials," *J. Phys. A* **42**, 275306 (2009).
- ²⁰H. Schlichting, *Boundary-Layer Theory*, 7th ed. (McGraw Hill, New York, 1979).
- ²¹D. E. Coles, "The law of the wake in the turbulent boundary layer," *J. Fluid Mech.* **1**, 191 (1956).
- ²²R. J. Volino and M. P. Schultz, "Determination of wall shear stress from mean velocity and Reynolds shear stress profiles," *Phys. Rev. Fluids* **3**, 034606 (2018).
- ²³C. E. Brennen, *Internet Book on Fluid Dynamics* (Dankat Publishing, 2016).
- ²⁴L. P. Erm and P. N. Joubert, "Low-Reynolds-number turbulent boundary layers," *J. Fluid Mech.* **230**, 1–44 (1991).
- ²⁵B. Brzek, R. Bayoan Cal, G. Johansson, and L. Castillo, "Inner and outer scalings in rough surface zero pressure gradient turbulent boundary layers," *Phys. Fluids* **19**, 065101 (2007).
- ²⁶H. S. Shafi and R. A. Antonia, "Anisotropy of the Reynolds stresses in a turbulent boundary layer on a rough wall," *Exp. Fluids* **18**(3), 213–215 (1995).
- ²⁷P. R. Spalart, "Direct simulation of a turbulent boundary layer up to $R_0 = 1410$," *J. Fluid Mech.* **187**, 61 (1988).
- ²⁸M. Inoue, "Large-eddy simulation of the flat-plate turbulent boundary layer at high Reynolds numbers," Ph.D. thesis, California Institute of Technology, 2012.
- ²⁹J. Kim, P. Moin, and R. Moser, "Turbulence statistics in fully developed channel flow at low Reynolds number," *J. Fluid Mech.* **177**, 133–166 (1987).
- ³⁰L. Landau and E. Lifchitz, *Statistical Physics* (Pergamon Press, Oxford, 1987).
- ³¹A. A. Townsend, "The properties of equilibrium boundary layers," *J. Fluid Mech.* **1**, 561–573 (1956).
- ³²H. P. Bakewell, Jr. and J. L. Lumley, "Viscous sublayer and adjacent wall region in turbulent pipe flow," *Phys. Fluids* **10**, 1880–1889 (1967).
- ³³M. Uhlman, "Turbulences flows and their modeling," www.ifh.uni-karlsruhe.de/people/uhlmann (2008).
- ³⁴J. Jimenez, S. Hoyas, M. P. Simens, and Y. Mizuno, "Turbulent boundary layers and channels at moderate Reynolds numbers," *J. Fluid Mech.* **657**, 335–360 (2010).
- ³⁵J. A. Businger *et al.*, "Flux profile relationships in the atmospheric surface layer," *J. Atmos. Sci.* **28**, 181–189 (1971).
- ³⁶P. A. Sheppard, "The aerodynamic drag of the Earth's surface and the value of Karman's constant in the lower atmosphere," *Proc. R. Soc. London Ser. A* **188**, 208–222 (1947).
- ³⁷M. Lee and R. Moser, "Direct numerical simulation of turbulent channel flow," *J. Fluid Mech.* **774**, 395–415 (2015).
- ³⁸Z. S. She, X. Chen, and F. Hussain, "Quantifying wall turbulence via a symmetry approach: A Lie group theory," *J. Fluid Mech.* **827**, 322–356 (2017).
- ³⁹N. R. Panchapakesan and J. L. Lumley, "Turbulence measurements in axisymmetric jets of air and helium. Part 1. Air jet," *J. Fluid Mech.* **246**, 197 (1993).
- ⁴⁰H. J. Hussein, S. P. Capp, and W. K. George, "Velocity measurements in a high-Reynolds-number, momentum-conserving, axisymmetric, turbulent jet," *J. Fluid Mech.* **258**, 31 (1994).
- ⁴¹J. A. Sillero, J. Jimenez, and R. D. Moser, "One-point statistics for turbulent wall-bounded flows at Reynolds numbers up to 2000," *Phys. Fluids* **25**, 105102 (2013).
- ⁴²A. G. Gungor, Y. Maciel, M. P. Simens, and J. Soria, "Analysis of a turbulent boundary layer subjected to a strong adverse pressure gradient," *J. Phys.* **506**, 012007 (2014).
- ⁴³S. L. Tang and R. A. Antonia, "Similarity for dissipation wall turbulence," *J. Fluid Mech.* **960**, A18 (2023).